## General Disclaimer

## One or more of the Following Statements may affect this Document

- This document has been reproduced from the best copy furnished by the organizational source. It is being released in the interest of making available as much information as possible.

- This document may contain data, which exceeds the sheet parameters. It was furnished in this condition by the organizational source and is the best copy available.

- This document may contain tone-on-tone or color graphs, charts and/or pictures, which have been reproduced in black and white.

- This document is paginated as submitted by the original source.

- Portions of this document are not fully legible due to the historical nature of some of the material. However, it is the best reproduction available from the original submission.

# NASA Contractor Report 168103



# Testing of Felt - Ceramic Materials for Combustor Applications

**R.S. Venkat Raman and Gerald Roffe**
*General Applied Science Laboratories, Inc.*
*Westbury, New York*

**Prepared for**
**Lewis Research Center**
**under Contract NAS3-22775**

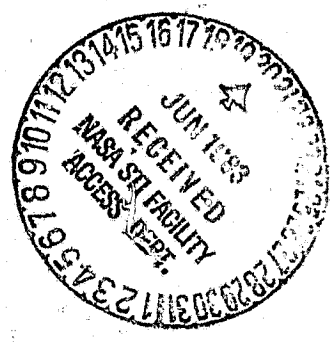


**April 1983**

| 1. Report No. | 2. Government Accession No. | 3. Recipient's Catalog No. |
|---|---|---|
| NASA CR-168103 | | |

| 4. Title and Subtitle | 5. Report Date |
|---|---|
| Testing of Felt-Ceramic Materials for Combustor Applications | 6. Performing Organization Code |

| 7. Author(s) | 8. Performing Organization Report No. |
|---|---|
| R.S. Venkat Raman and Gerald Roffe | 10. Work Unit No. |

| 9. Performing Organization Name and Address | 11. Contract or Grant No. |
|---|---|
| General Applied Science Laboratories, Inc.<br>Merrick and Stewart Avenues<br>Westbury, NY 11590 | NAS3 - 22775 |



| 12. Sponsoring Agency Name and Address | 13. Type of Report and Period Covered |
|---|---|
| U.S. Army Research & Technology Laboratories (AVRADCOM)<br>Propulsion Laboratory and<br>NASA Lewis Research Center<br>Cleveland, OH 44135 | Contractor Final Report |
| | 14. Sponsoring Agency Code<br>1L162209AH76 |

15. Supplementary Notes

Project Manager, David B. Ercegovic, U.S. Army Research & Technology Laboratories (AVRADCOM)
Propulsion Laboratory
Lewis Research Center
Cleveland, OH 44135

16. Abstract

The feasibility of using composite felt-ceramic materials as combustor liners was experimentally studied. The material consists of a porous felt pad sandwiched between a layer of ceramic and one of solid metal. Flat, rectangular test panels, which encompassed several design variations of the basic composite material, were tested, two at a time, in a premixed gas turbine combustor as sections of the combustor wall.

Tests were conducted at combustor inlet conditions of 0.5 MPa and 533K with a reference velocity of 25 m/s. The panels were subjected to a hot gas temperature of 2170K with 1% of the total airflow used to film cool the ceramic surface of the test panel.

In the first phase of testing, combustor operating conditions were maintained for 3 minutes followed by a shutdown. This sequence was repeated 4 times in quick succession for all panels. Other than a slight discoloration of both the ceramic and back surfaces, the panels revealed no signs of deterioration.

In the second phase, two of the panels underwent further cyclic testing. Here, combustor operating conditions were maintained for 2 minutes followed by a shutdown. This sequence was repeated 30 times. Following completion of this test sequence, one of the panels exhibited small non-catastrophic mudflat cracks on the ceramic surface, while the other had partial separation at the felt-ceramic interface.

In general, thin ceramic layers yield low ceramic stress levels with high felt-ceramic interface temperatures. On the other hand, thick ceramic layers result in low felt-ceramic interface temperatures but high ceramic stress levels. Extensive thermal cycling appears to cause material degradation, but for a limited number of cycles, the survivability of felt-ceramic materials, even under extremely severe combustor operating conditions, was conclusively demonstrated.

| 17. Key Words (Suggested by Author(s)) | 18. Distribution Statement |
|---|---|
| Felt-Ceramic<br>Felt Pad<br>Premixed Combustor<br>Ceramic Combustor<br>Ceramic Liner | Unclassified - Unlimited<br>STAR Category 07 |



| 19. Security Classif. (of this report) | 20. Security Classif. (of this page) | 21. No. of Pages | 22. Price* |
|---|---|---|---|
| Unclassified | Unclassified | | |

* For sale by the National Technical Information Service, Springfield, Virginia 22161

TABLE OF CONTENTS

## LIST OF TABLES

## LIST OF FIGURES

## LIST OF FIGURES (cont'd.)

## INTRODUCTION

A new composite material is being developed jointly by the U.S. Army and NASA for use in gas turbine combustion chambers. The material, designated "Felt-Ceramic," consists of a solid metal base, a porous or felt-metal intermediate layer and a ceramic surface layer. The solid metal base provides the necessary strength while the ceramic surface layer allows the material to withstand very high surface temperatures. The felt-metal intermediate layer is designed to yield at relatively low levels of stress, thereby absorbing the differential expansion which develops between the solid metal and the ceramic as the material is heated.

This report describes a series of tests conducted on a number of design variations of the felt ceramic composite material under conditions representative of gas turbine combustor operation. The material samples were installed as wall sections in a premixed combustor which provided a uniform flow of combustion gas at a temperature of 2170 K and a pressure of 0.5 MPa. The samples were subjected to steady, unsteady, and cyclic loads of both a mechanical and thermal nature. The samples were then evaluated based on their thermal and mechanical performance.

## APPARATUS AND PROCEDURES

The gas turbine combustion test rig used in this program is shown in Figure 1. The rig is a segment of a large annular combustor and produces a premixed propane/air flame stabilized by a perforated plate flameholder. The hot section is 100mm x 100mm with film-cooled liner sections as the top and bottom sections and ceramic-coated water-cooled sidewalls. Entrance temperature and pressure are measured just upstream of the Figure 1 inlet station and exit conditions are measured in an exhaust instrumentation spool mounted immediately downstream of the combustor.

The combustor section is shown schematically in Figure 2, which illustrates the placement of the felt-ceramic test panels. Air enters the combustor assembly through a $6^{o}$-half angle dump diffuser and is divided between the mixture preparation duct and the bypass duct. Part of the air in the bypass duct feeds the variable cooling air plenum. The remaining bypass air passes over the back surface of the test panel and enters the combustor hot section through either the film cooling slots or the dilution holes. A very small fraction of the bypass air enters the combustor through a series of holes drilled through the upstream and downstream edges of the test panels.

The amount of air entering the variable cooling plenum is controlled by a shutter mechanism which is actuated by an externally-mounted motor. The shutter mechanism is capable of admitting up to 2% of the total air to the variable cooling plenum. This plenum feeds the film cooling slot located immediately upstream of the test panel. The cooling plenum is completely sealed so the air that enters through the shutter mechanism exits through the cooling slot without any loss.

The shutter mechanism is shown in Figure 3. The shutter is comprised of a disc with two circumferential slots which rotates to expose series of holes drilled through to the plenum. To minimize leakage, the shutter is held against the plenum by a heavy spring. Depending on the angular position of the shutter, 0,2,4,6 or 8 holes are opened, allowing 0%, 0.5%, 1.0% 1.5%, or 2% of the total combustor airflow to enter each cooling plenum.

The flameholder is a square plate 25mm thick with twenty-five equally

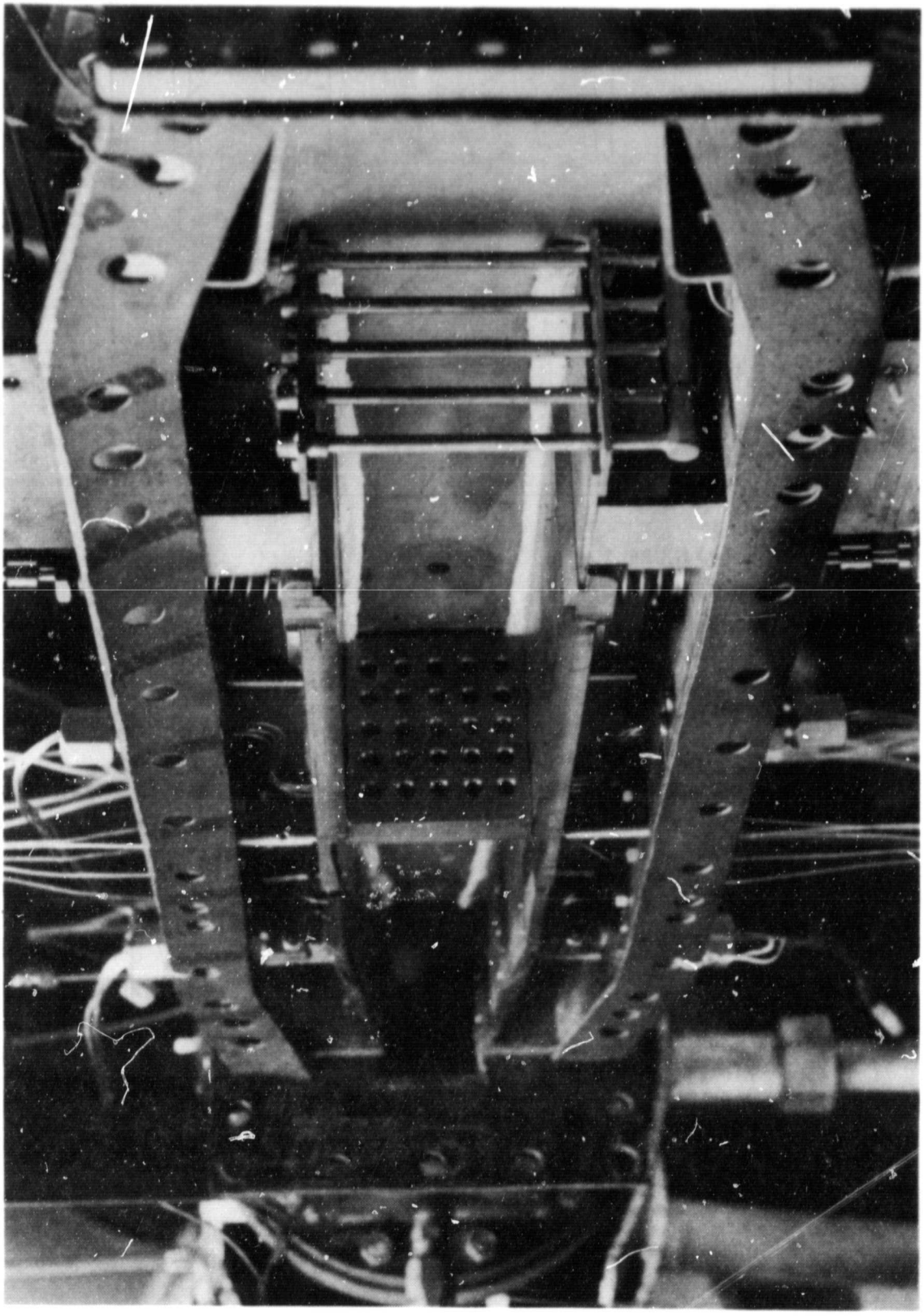

FIGURE 1. PHOTOGRAPH OF TEST COMBUSTOR

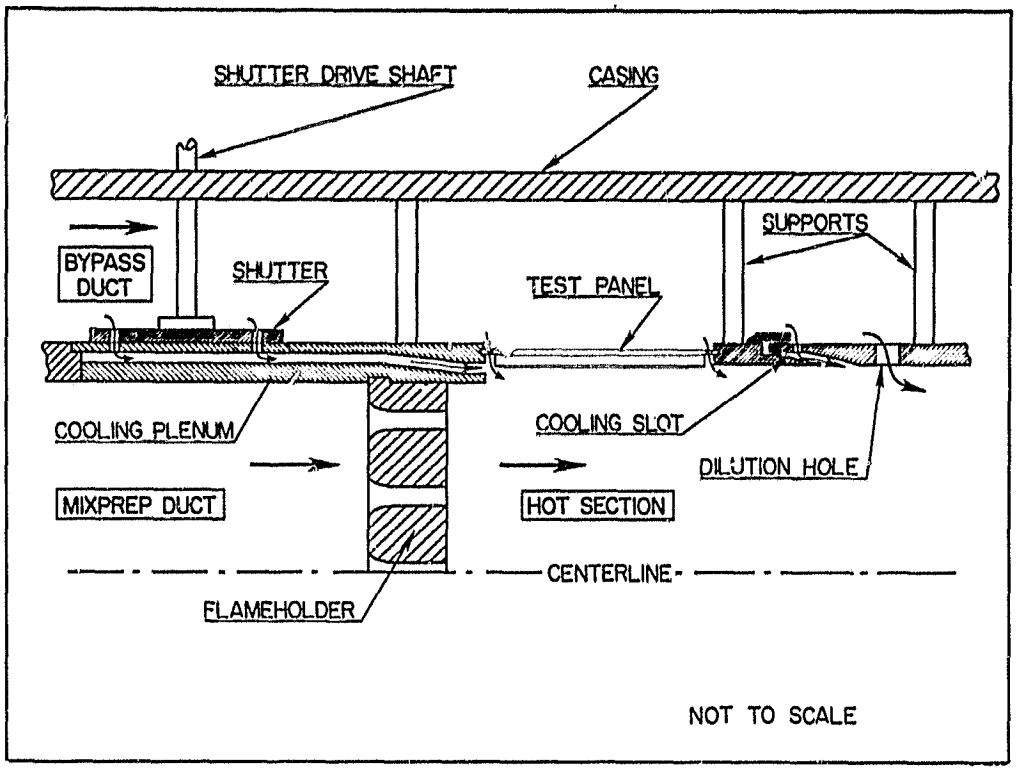


FIGURE 2. TEST RIG DETAILS



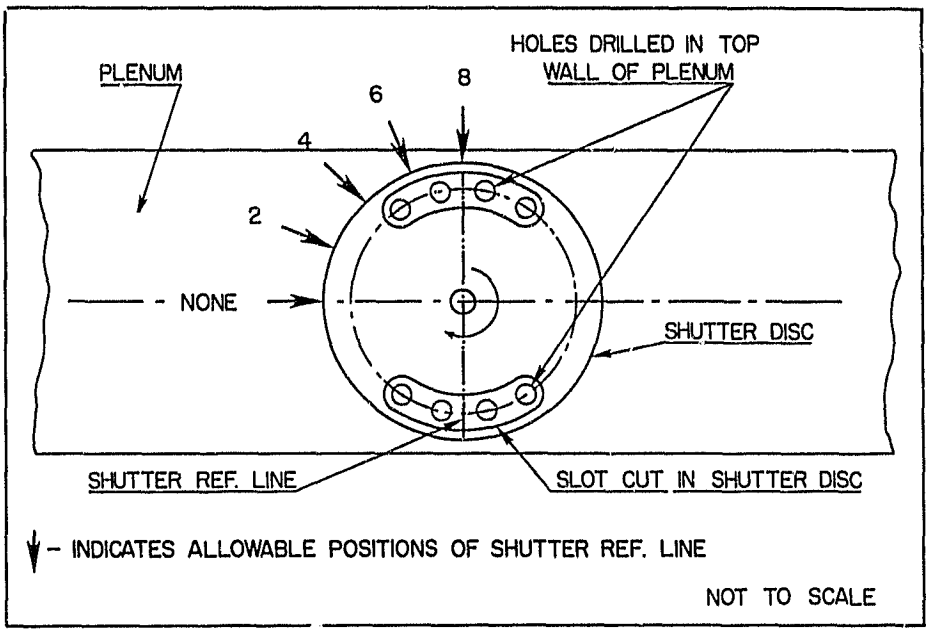


FIGURE 3. VARIABLE COOLING AIR MECHANISM

spaced holes 6.9mm in diameter. The hole passage are rounded on the entrance side to avoid local flow separation. The flameholder produces a geometric blockage of 90%.

The details of the fuel system are illustrated schematically in Figure 4. Liquid propane is stored in a reservoir which is pressurized by gaseous nitrogen. The fuel is withdrawn near the bottom of the reservoir and passed through a turbine flowmeter, a pressure regulator and a cavitating venturi. This produces a fuel flow rate that is determined by the regulator loading pressure and is independent of pressure fluctuations in the combustor. The fuel is then passed through a heat exchanger which heats the propane to 370K, slightly above its critical temperature. A thermocouple and pressure tap located in the propane feed plenum are monitored to ensure that the fuel being injected into the combustor is in the gaseous state.

Figure 4 also illustrates the fuel injector assembly, which consists of five 6.4mm diameter tubes connected to a 12.7mm diameter feed plenum. Each tube has five 1.1mm diameter injection ports giving a total of twenty-five ports. These ports, which inject fuel in the co-stream direction, are evenly distributed across the cross-section of the mixture preparation duct.

The size and basic construction of the felt-ceramic test panels are illustrated in Figure 5. The back surface is made of Inconel alloy 718 and is 0.8mm (.032 in.) thick. The felt pad material, density, and thickness change from panel to panel, and are listed in Table I. The felt pad is brazed to the back surface and the opposite side is plasma sprayed with a NiCrAlY bond coat after being roughened by grit blasting with aluminum oxide. The thickness of the NiCrAlY coating is approximately 0.13mm (0.005 in.). The coated surface is then plasma-sprayed with yttria-stabilized zirconia ceramic. The percentage of yttria and the thickness of the ceramic are different for different panels, and are listed in Table I. Some panels (identified in Table I) are transpiration cooled using holes which extend through the ceramic to the back surface. The cooling hole

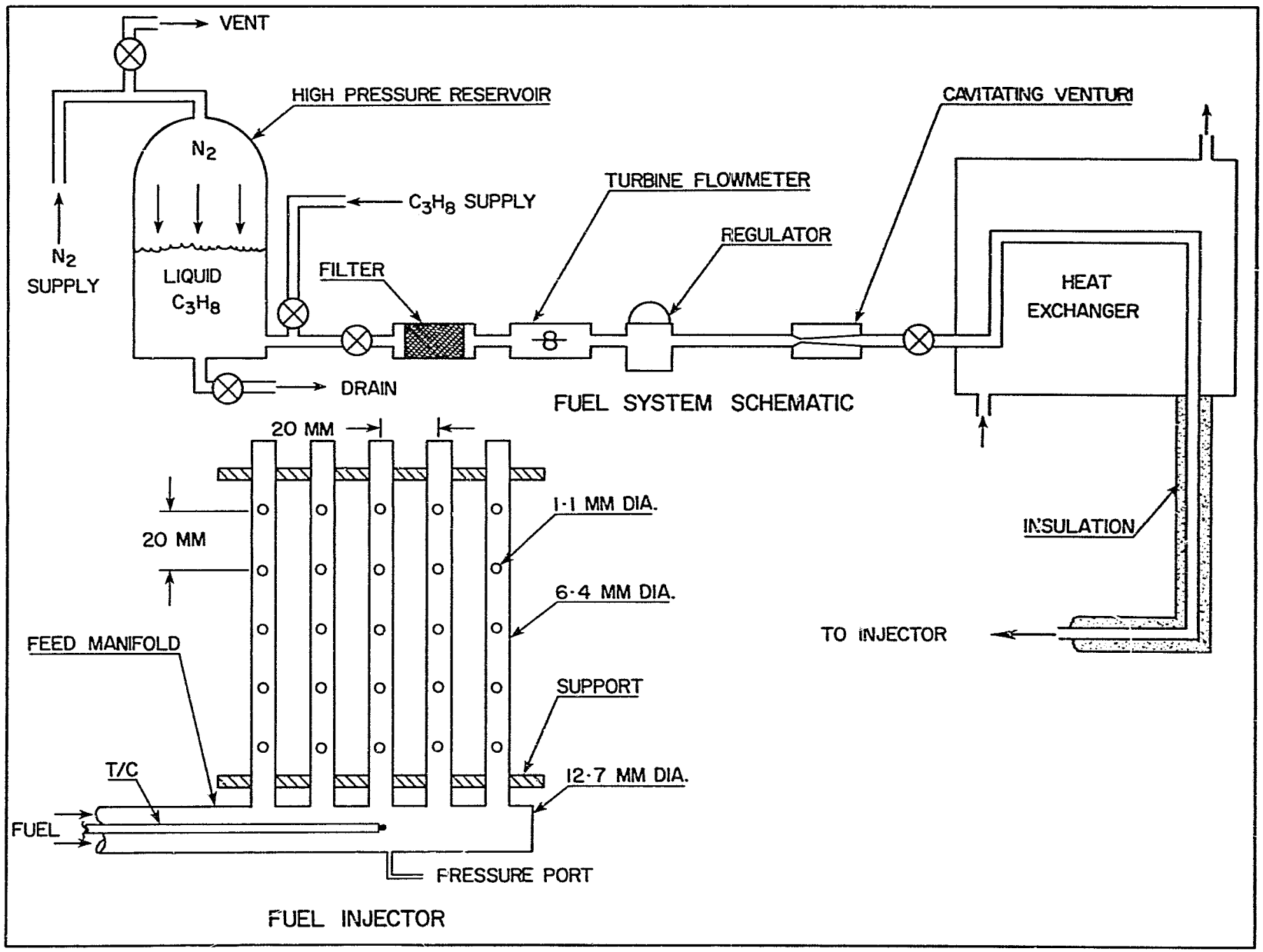


FIGURE 4. FUEL SYSTEM SCHEMATIC AND FUEL INJECTOR DESIGN

| PANEL NO. | PAD MATERIAL | PAD DENSITY (%)*** | PAD THICKNESS (mm) | CERAMIC MATERIAL (% Y)** | CERAMIC THICKNESS (mm) | THERMO-COUPLE PATTERN |
|---|---|---|---|---|---|---|
| 16104-4 | H-875 | 35 | 3.81 | 20 | 1.91 | [illegible] |
| 16104-5 | H-875 | 35 | 3.81 | 20 | 3.30 | [illegible] |
| 16104-7 | H-875 | 35 | 2.54 | 20 | 1.91 | Y |
| 16104-8 | H-875 | 35 | 2.54 | 20 | 3.30 | Z |
| 16104-10 | H-875 | 35 | 2.54 | 8 | 1.91 | Y |
| 16104-11 | H-875 | 45 | 2.54 | 20 | 1.91 | Y |
| 16104-12 | H-875 | 45 | 2.54 | 20 | 3.30 | Y |
| 16104-14 | H-875 | 45 | 2.54 | 8 | 1.91 | Y |
| 16104-17 | H-875 | 45 | 3.81 | 20 | 1.91 | Y |
| 16104-18 | H-875 | 45 | 3.81 | 20 | 3.30 | Y |
| 16104-42 | H-875 | 45 | 3.81 | 8 | 1.91 | Y |
| 16656-2* | H-875 | 35 | 2.54 | 20 | 1.91 | X |
| 16656-3* | H-875 | 35 | 2.54 | 20 | 1.91 | X |
| 16656-4* | H-875 | 35 | 2.54 | 20 | 1.91 | X |
| 16656-5* | H-875 | 35 | 2.54 | 8 | 1.91 | X |
| 16104-19 | H-534 | 42 | 3.81 | 20 | 1.91 | Y |
| 16104-20 | H-534 | 42 | 3.81 | 20 | 3.30 | Y |
| 16104-21 | H-534 | 32 | 3.81 | 20 | 1.91 | Y |
| 16104-22 | H-534 | 32 | 3.81 | 20 | 3.30 | Z |
| 16104-23 | H-534 | 42 | 3.81 | 8 | 1.91 | Y |
| 16104-28 | H-534 | 32 | 2.54 | 20 | 1.91 | Z |
| 16104-29 | H-534 | 32 | 2.54 | 20 | 3.30 | Y |
| 16104-30 | H-534 | 32 | 2.54 | 8 | 1.91 | Y |
| 16104-33 | H-534 | 42 | 2.54 | 20 | 1.91 | Y |
| 16104-35 | H-534 | 42 | 2.54 | 20 | 3.30 | Y |
| 16104-36 | H-534 | 42 | 2.54 | 8 | 1.91 | Y |
| 16656-8* | H-534 | 32 | 2.54 | 20 | 1.91 | X |
| 16656-9* | H-534 | 32 | 2.54 | 20 | 1.91 | X |
| 16656-10* | H-534 | 32 | 2.54 | 20 | 1.91 | X |
| 16656-11* | H-534 | 32 | 2.54 | 8 | 1.91 | X |

* Transpiration cooled

** % Yttria in Yttria stabilized Zirconia

***% Solidity

TABLE 1. DESIGN DETAILS OF THE TEST PANELS

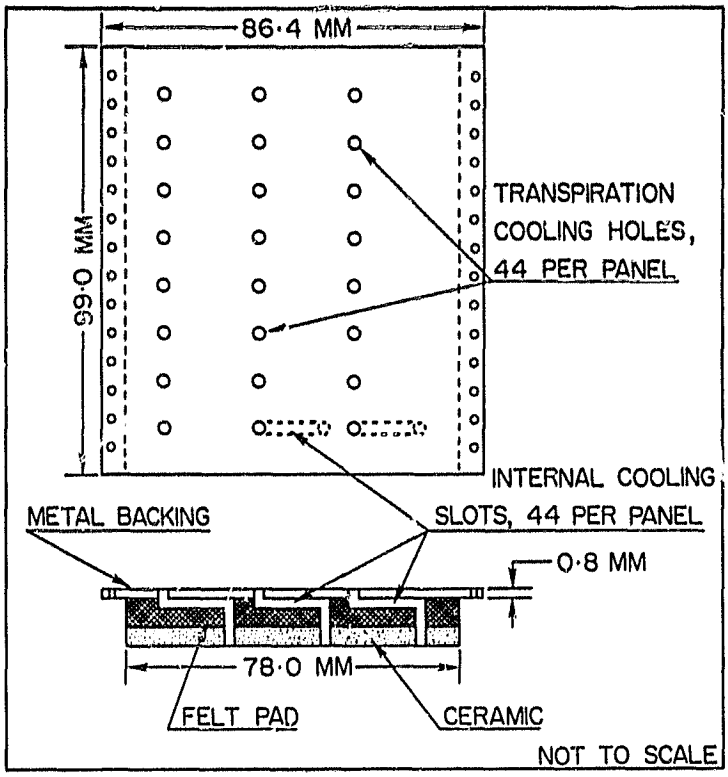


FIGURE 5. TEST PANEL DESIGN

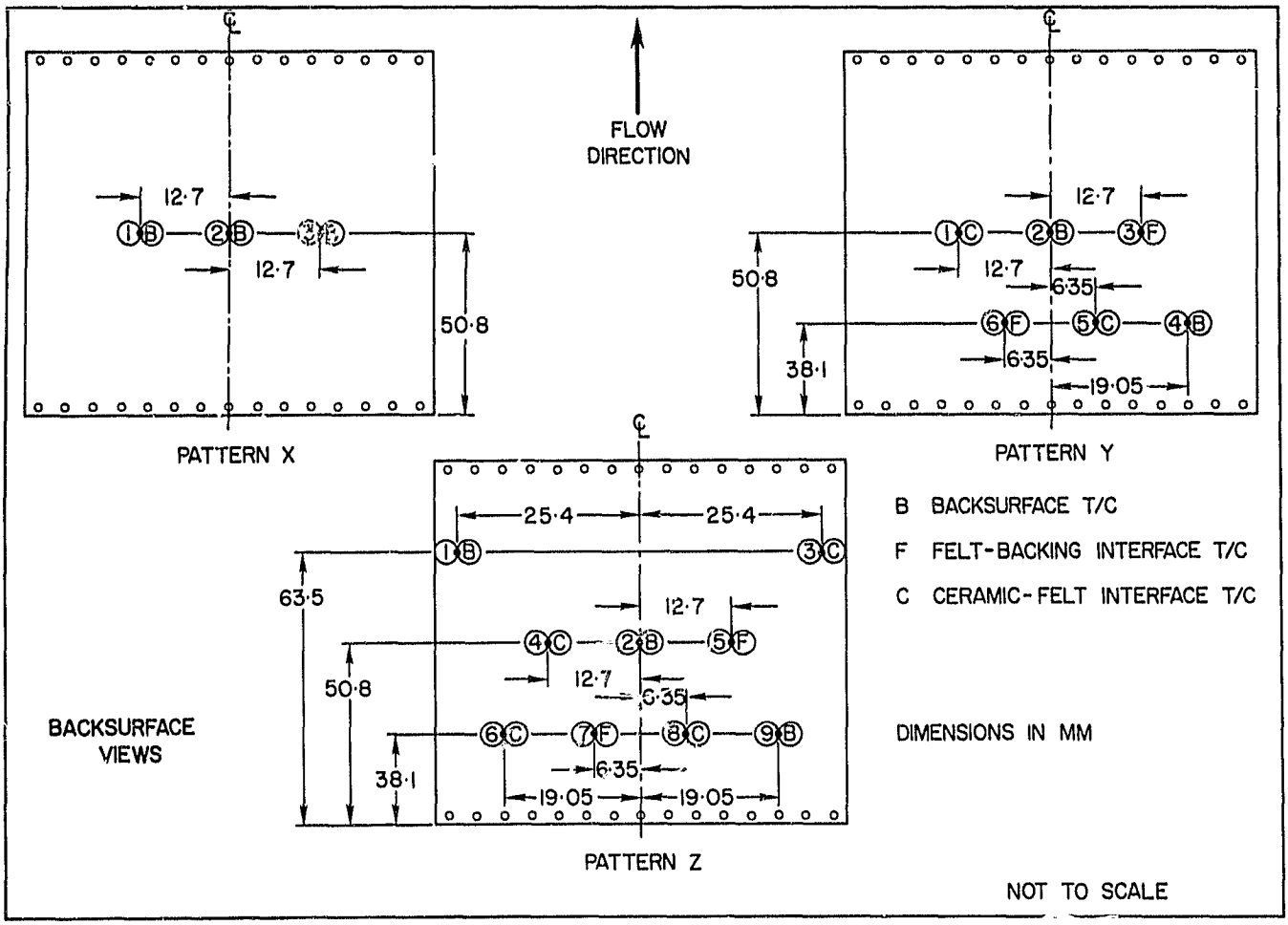


FIGURE 6. TEST PANEL INSTRUMENTATION LAYOUT

pattern is illustrated in Figure 5. The test panels are instrumented with thermocouples using the three patterns illustrated in Figure 6. The particular pattern used for any given panel is listed in Table 1.

The test panels are mounted in the combustor section with their leading edges 70mm downstream of the flameholder exit plane as illustrated in Figure 7. The panel is supported by grooves in the adjoining combustor liner sections and is sealed to the sidewall by a thin layer of compressed fiberfrax. The panel thermocouples exit the rig through individual compression seals attached to a removable plate in the combustor pressure casing.

The transpiration cooled panels were tested in an atmospheric test stand to determine the pressure drop across them for various transpiration air flow rates. The test stand is illustrated schematically in Figure 8. Cold air is admitted to the test stand through a venturi. Stagnation temperature and pressure are measured upstream of the venturi as well as static pressure at the venturi throat. After entering the test stand, the air passes through a series of screens before reaching the test panel. The pressure drop across the plate is measured with a differential pressure gauge. The panels are mounted so that the flow of air is from back to front. The entire panel sits on a ledge cut in the end flange and is sealed against the ledge with a soft gasket. The panel is held against the end flange by two brackets which bolt on to the end flange. The brackets hold the backing of the panels along the edges which contain the small slave cooling holes. This mounting technique seals all four edges of the test panel, including the slave cooling holes, and avoids placing external mechanical stress on the composite portion of the test panels.

The felt ceramic panels were tested at a pressure of 0.5 MPa with an inlet-air temperature of 533K and an adiabatic flame temperature of 2170K corresponding to a primary zone equivalence ratio of 0.93. The differential pressure across the panels was 16.3 kPa. The combustor reference velocity was 25 m/s. The panels were convectively cooled on their back surfaces by the bypass air with a velocity of 13.6 m/s and a temperature 493K. The panels were film cooled at their ceramic surfaces using 1.0% of the total

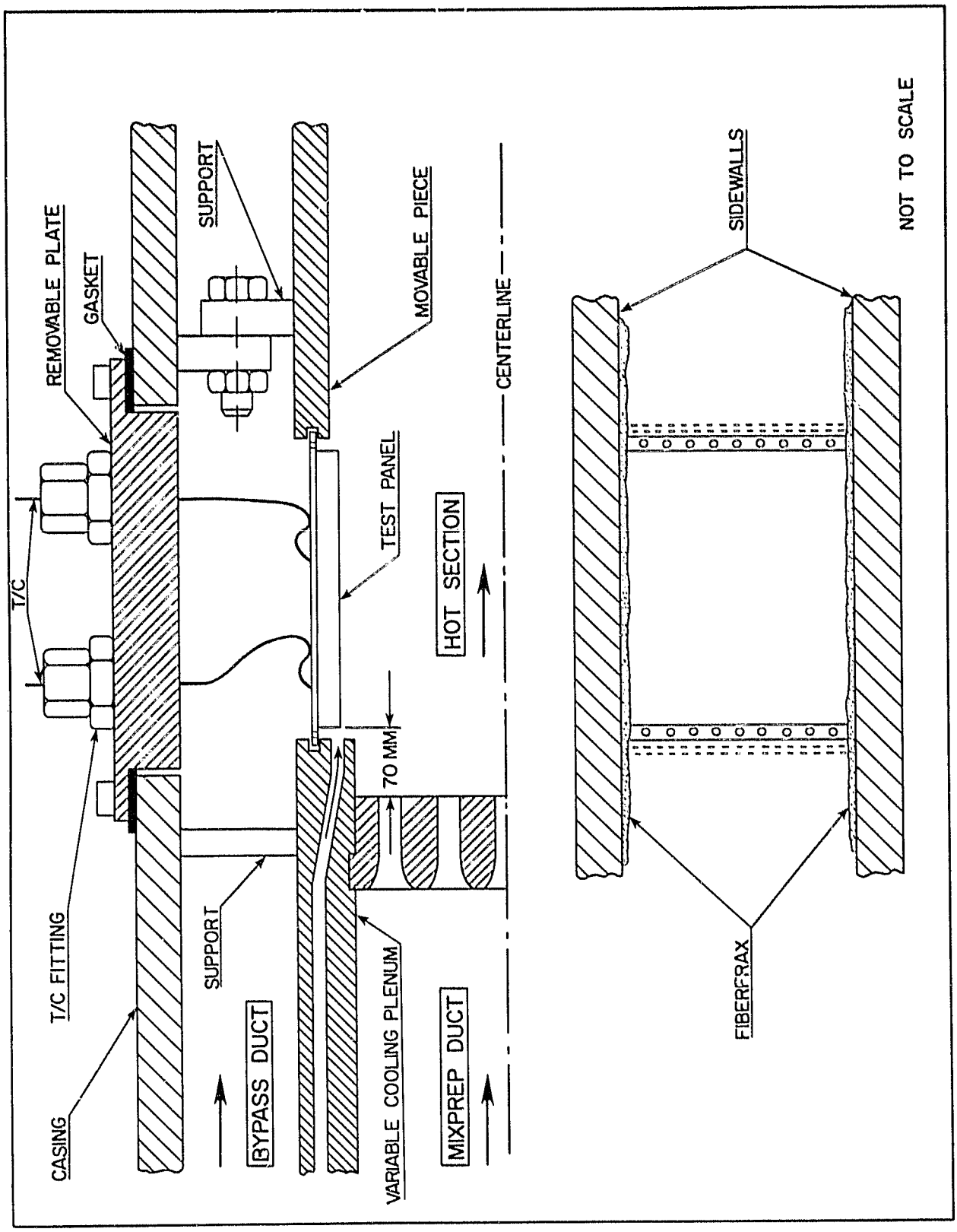


FIGURE 7. TEST PANEL INSTALLATION DETAILS

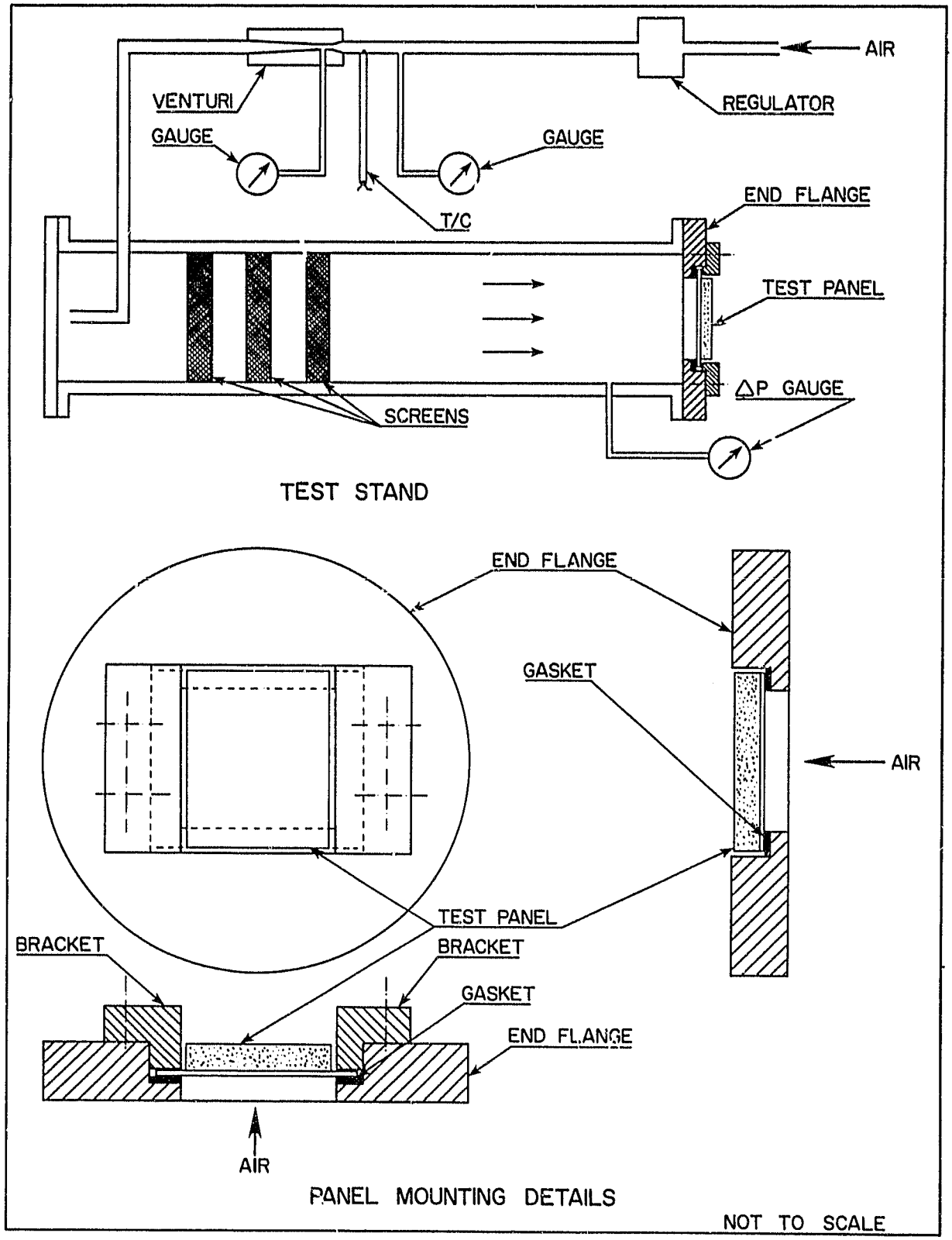


FIGURE 8. ATMOSPHERIC TEST STAND AND PANEL MOUNTING DETAILS

entrance airflow. The variable cooling air slot which provides this was incorporated in the combustor because of the possibility that some felt ceramic panels would not survive the severe flame temperature of 2170K without significant film coolant. As it turned out, the ceramic surfaces of these panels did not need any film cooling. However, the cooling slot itself, which was made of stainless steel, showed signs of melting with 0% coolant flow. So, a small amount, 1% of the total combustor airflow, was used to protect the cooling slot. A complete listing of test conditions is presented in Table 2.

The only departure from the conditions of Table 2 is the primary zone equivalence ratio for the transpiration cooled panels. For these panels, the transpiration coolant flow, in principle, reduces the relative amount of air in the primary zone. Therefore, in order to maintain the same primary zone equivalence ratio for these panels as for the others, the fuel flow rate was slightly reduced. However, the data later revealed that the transpiration coolant flow had no measurable effect on the relative amount of air in the primary zone. But, since the fuel flow rate was reduced, the primary zone equivalence ratio for the transpiration cooled panels turned out to be $.88 \pm 02$. All other conditions, including the differential pressure across the panels, were the same as those listed in Table 2.

Combustion testing of the panels was divided in two parts: screening tests and endurance tests. In the screening tests, the conditions of Table 2 were maintained for 3 minutes, followed by a shutdown. The shutdown procedure involved an abrupt fuel shut-off to provide the greatest possible thermal shock, followed by a gradual cessation of air flow. This sequence was repeated four times. Figure 9 shows temperature traces for a typical screening test. The temperature numbers in this figure correspond to the thermcouples in Pattern Y. The four test cycles of the screening test can be clearly identified in the figure.

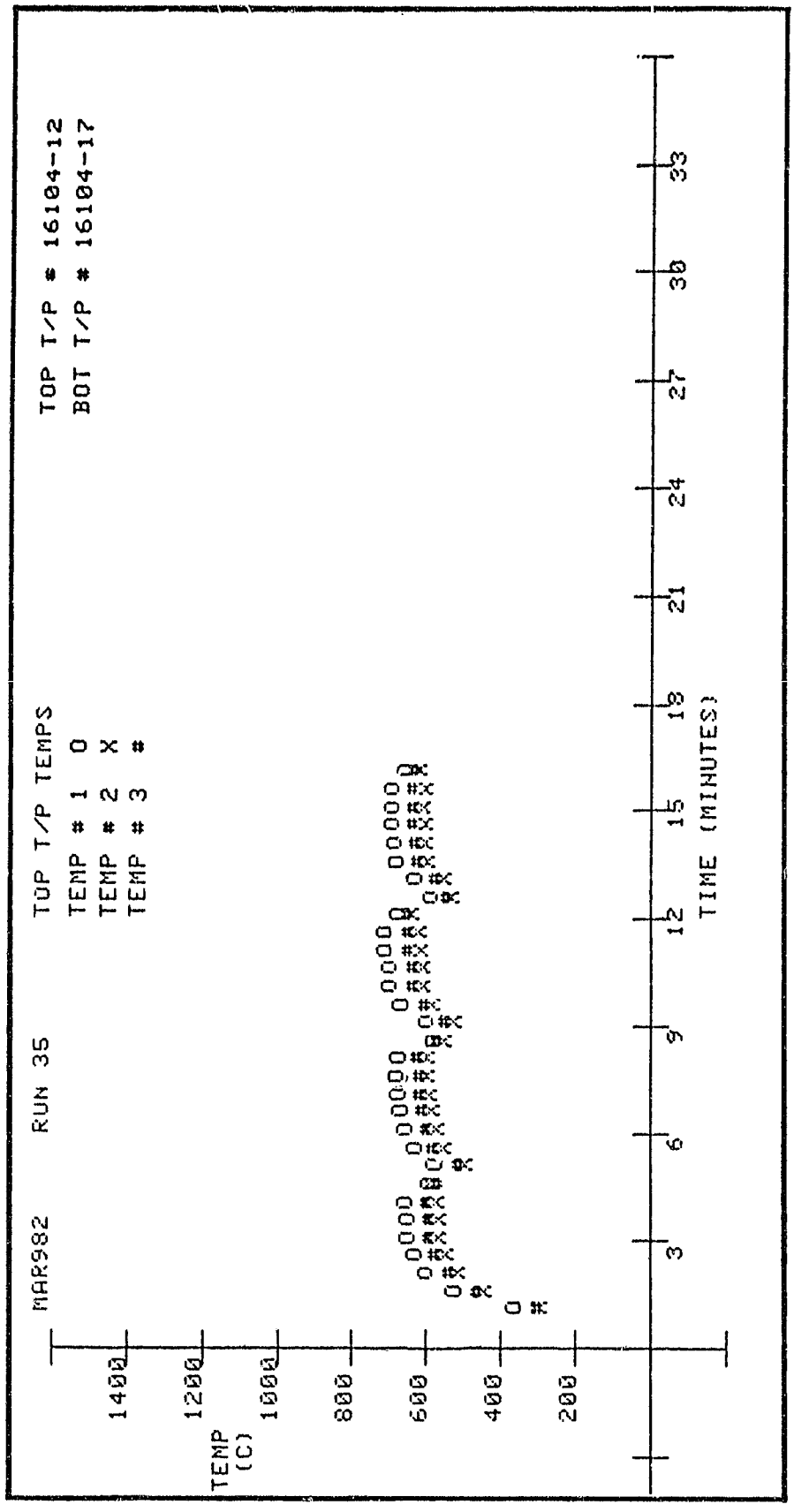


FIGURE 9. TYPICAL SCREENING TEST RECORD OF TEST PANEL THERMOCOUPLES.

| | | |
|---|---|---|
| Combustor inlet temperature | = | 533 ± 12K |
| Combustor reference velocity | = | 25 m/s |
| Combustor inlet pressure | = | 0.5 + .02 MPa |
| Total air flow rate | = | 0.83 ± .02 kg/s |
| Primary air flow rate | = | 48% of total |
| | = | 0.40 kg/sec |
| Total bypass duct air flow | = | 0.215 kg/s (each duct) |
| Back surface coolant temp. | = | 493 ± 12K |
| Mean back surface coolant vel. | = | 13.6 m/s |
| Ceramic coolant flow rate | = | 0.010 x 0.83 kg/s |
| Mean ceramic coolant velocity | = | 11.6 m/s |
| Differential pressure across panel | = | 16.3 ± 2 kPa |
| Overall pressure drop in combustor | = | 30.6 ± 2 kPa |
| Primary zone equivalence ratio | = | 0.93 ± .015 |
| Adiabatic flame temp. | = | 2170 ± 35K |

TABLE 2. TEST CONDITIONS

Endurance testing was similar to screening testing except that the firing sequences were 2 minutes each, and a total of thirty sequences were run. The firing sequences were run six at a time separated by a nominal interval of 1 minute. Five such multiple sequence run sets were made with an interval of 24 hours between each set.

## RESULTS AND DISCUSSION

### Combustion Efficiency

While the combustor was operating at the described conditions, gas samples were extracted from the exit rake and analyzed. The analyses yielded carbon monoxide levels of 850±50 parts per million which indicated a combustion efficiency of better than 99%. No measurable hydrocarbon levels were detected in any of the samples analyzed.

### Flow Split

The geometric flow split, that is the ratio of the primary zone or mixture preparation flow rate to the total flow rate, based on flow areas is 0.48. This ratio can also be obtained during combustor operation by using the fuel as a tracer gas and measuring both the primary and overall fuel-air ratios. The overall fuel-air ratio is obtained from a gas analysis of the exhaust gas sample, and the primary fuel-air ratio is obtained by measuring the $CO_2$ concentration in the primary gas sample after it has undergone catalytic combustion. The flow split is then the ratio of the overall fuel-air ratio to the primary zone fuel-air ratio. This chemically obtained flow split varied from .44 to .52 which is within ± 10% of the theoretically obtained flow split. The theoretical value of 0.48 is used in all computations.

### Spanwise Temperature Uniformity

Prior to conducting the screening tests, a temperature uniformity test was performed. In this test, hot side temperatures were measured along the spanwise centerline of a stainless steel panel. This panel, shown in Figure 10, has the same dimensions as the felt-ceramic specimens and is instrumented with thermocouples in such a manner that the thermocouple beads are flush with the hot side surface of the panel. Two such panels, one on the top and another on the bottom, were installed in the combustor for the test.

The spanwise temperature uniformity test was conducted with the variable cooling air slot set at its maximum value of 2%. The maximum primary zone equivalence ratio that could be reached during this test without distressing the stainless

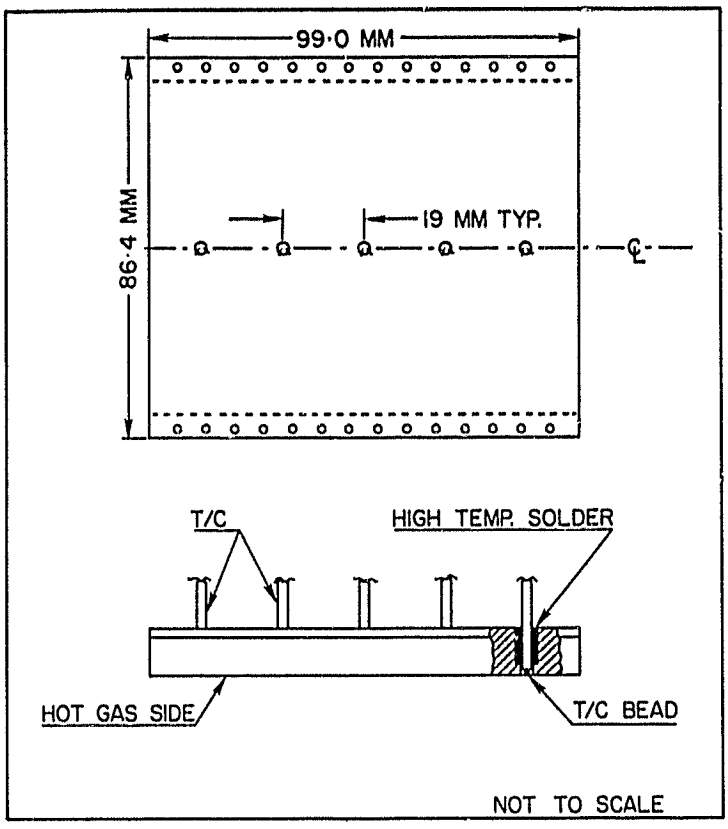


FIGURE 10. TEST PANEL USED FOR DETERMINING SPANWISE TEMPERATURE DISTRIBUTION

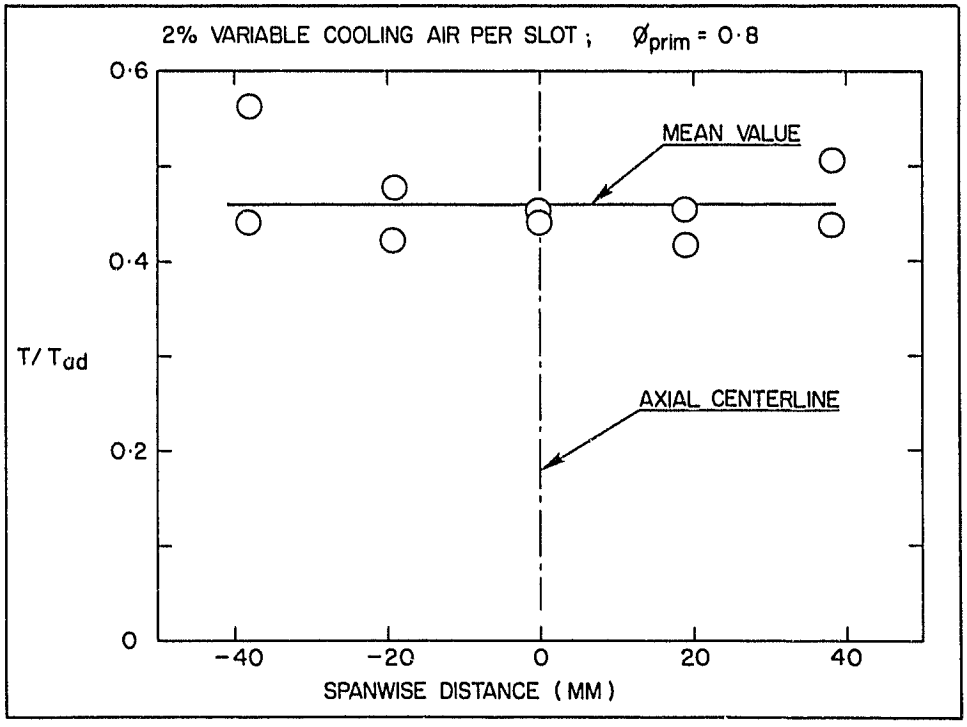


FIGURE 11. SPANWISE TEMPERATURE DISTRIBUTION

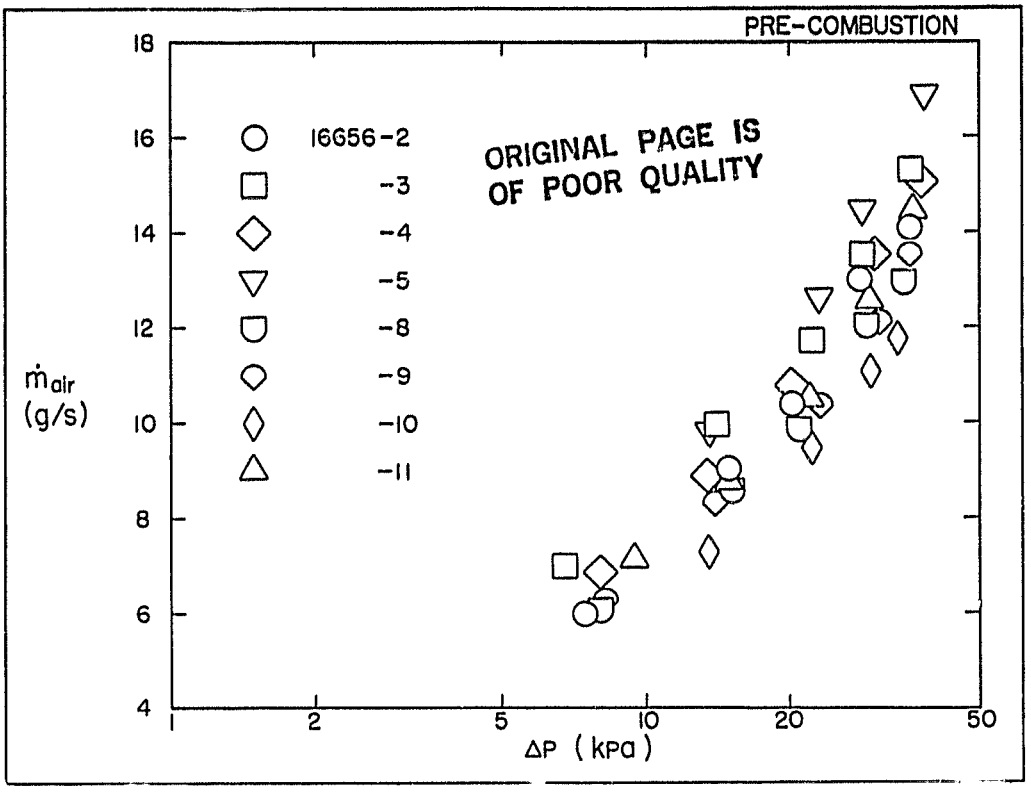


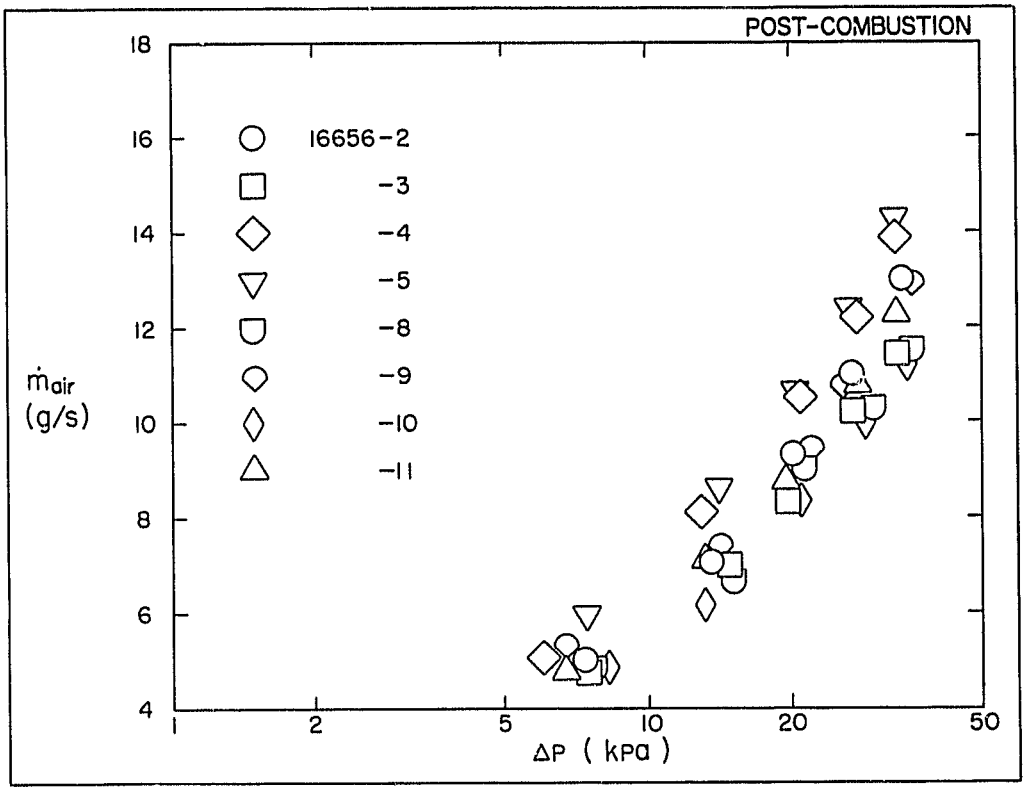


FIGURE 12. FLOW CHARACTERISTICS OF TRANSPIRATION COOLED PANELS

steel panels was 0.80. The measured temperatures for this condition are shown in Figure 11. These temperatures are normalized with respect to the adiabatic flame temperature, which was 1990K. The hot gas temperature distribution is relatively flat in the neighborhood of the axial centerline. The higher primary zone equivalence ratio of 0.93 and lower cooling air flow rate of 1% for the endurance and screening tests would be expected to produce a spanwise temperature distribution of even greater uniformity.

Pressure Drop

The flow characteristics of the eight transpiration cooled panels, identified in Table 1, were measured in an atmospheric discharge test stand both before and after undergoing screening tests. The mass flow results are shown in Figure 12. The various panels were all designed to yield the same mass flow rate for a given pressure drop. This design goal is essentially verified by the results and, as expected, the measured mass flow rate is proportional to the square root of the pressure drop. A slight decrease in the mass flow rate of all panels is observed after undergoing combustion testing. This is due to oxidation of the felt pad material which tends to reduce its porosity.

Screening Tests

The operating conditions for the screening tests, discussed earlier, are given in Table 2. After the screening tests, except for discoloration of the ceramic and back surfaces, none of the panels showed any visible evidence of failure. There were no mudflat cracks, felt-ceramic separations, or felt-backing separations for any of the panels. The ceramic surfaces of all the panels, after the screening tests, are shown in Figure 13. The black-grey material on the ceramic surfaces of panels 16104-7 and 16104-10 is a slag deposition from a flameholder burnout which occurred during an aborted screening test of these panels. The combustor rig was then repaired and these panels retested.

The temperatures recorded by the various thermocouples at steady state are listed in Table 3 for each panel. The thermocouple locations are shown in Figure 6. It should be noted that some back surface temperatures are higher

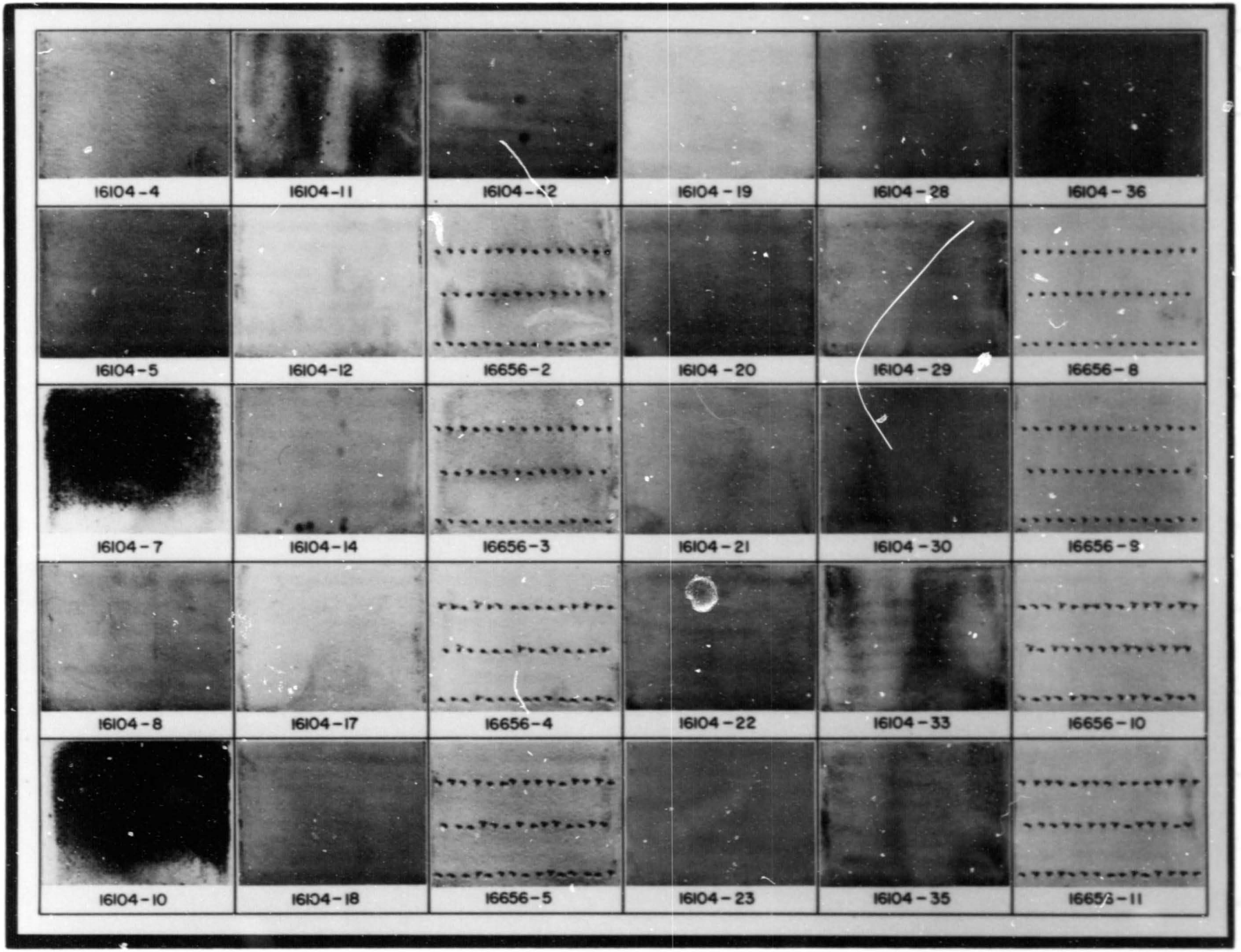


FIGURE 13. CERAMIC SURFACES OF ALL PANELS AFTER SCREENING TESTS

| T/C | 1 | 2, 2*† | 3 | 4, 1*† | 5, 3*† | 6 | 7, 6* | 8, 5* | 9, 4* |
|---|---|---|---|---|---|---|---|---|---|
| TYPE | B | B | C | C | F | C | F | C | B |
| | | | | | | | | | |
| 16104-8 | 833 | 855 | 1002 | 922 | 705 | 783 | 770 | 993 | - |
| 16104-22 | 867 | 765 | 736 | 907 | 691 | 896 | 749 | 835 | 693 |
| 16104-4 | 783 | 842 | 1040 | 741 | 744 | 620 | 667 | 1076 | - |
| 16104-28 | 951 | 876 | 753 | 888 | 594 | 823 | 645 | 891 | 720 |
| 16104-7 | | 900 | | 921 | 910 | | 815 | 901 | 904 |
| 16104-10 | | 950 | | 873 | 739 | | 883 | 785 | 805 |
| 16104-29 | | 807 | | 729 | 755 | | 748 | 966 | 883 |
| 16104-35 | | 888 | | 1002 | 755 | | 885 | 903 | 707 |
| 16104-33 | | 843 | | 774 | 889 | | 650 | 977 | 933 |
| 16104-11 | | 937 | | 1072 | 825 | | 984 | 903 | 741 |
| 16104-12 | | 851 | | 930 | 879 | | 837 | 862 | 878 |
| 16104-17 | | 912 | | 864 | 841 | | 805 | 837 | 807 |
| 16104-19 | | 961 | | 1010 | 944 | | 837 | 1009 | 930 |
| 16104-21 | | 849 | | 1003 | 750 | | 735 | 955 | 752 |
| 16104-5 | | 783 | | 921 | 779 | | 655 | 963 | 765 |
| 16104-20 | | 827 | | 872 | 763 | | 732 | 844 | 768 |
| 16104-18 | | 856 | | 932 | 784 | | 787 | 986 | 827 |
| 16104-42 | | 1014 | | 957 | 834 | | 1036 | - | 788 |
| 16104-23 | | 953 | | 1050 | 833 | | 798 | 1075 | 938 |
| 16104-30 | | 950 | | 927 | 916 | | 848 | 819 | 825 |
| 16104-14 | | 927 | | 909 | 829 | | 910 | 885 | 957 |
| 16104-36 | | 829 | | 1012 | - | | 923 | 1003 | 848 |
| 16656-2 | | 552 | | 542 | 552 | | | | |
| 16656-3 | | 532 | | 526 | 538 | | | | |
| 16656-4 | | 541 | | 531 | 555 | | | | |
| 16656-5 | | 549 | | 536 | 553 | | | | |
| 16656-8 | | 530 | | 540 | 532 | | | | |
| 16656-9 | | 516 | | 519 | 512 | | | | |
| 16656-10 | | 520 | | 529 | 525 | | | | |
| 16656-11 | | 529 | | 536 | 524 | | | | |

* For panels with pattern Y (6 thermocouples)
† For panels with pattern X (3 thermocouples)
All thermocouples with pattern X are Type B.



TABLE 3. STEADY STATE TEMPERATURES RECORDED BY THE VARIOUS TEST PANEL THERMOCOUPLES

than some felt-ceramic interface temperatures. This is a reflection of the fact that the temperature gradient through some of the panels was comparable with the spanwise surface temperature gradients or the partial failure of interlayer thermocouples by bead separation from the interface.

Since none of the panels showed any visible signs of mechanical or thermal failure, a combination of theory and experiment was employed to rate the performance of the various panel designs. There are two principal areas critical to panel performance. The first is the felt-ceramic interface and the second is the ceramic layer itself.

Consider the felt-ceramic interface. The temperature of this interface governs the potential relative thermal expansion between the felt pad and caramic layers, the strength of both materials, the thermally induced surface stress on the ceramic, and the oxidation resistance of the felt. At the measured values of the felt-ceramic interface temperatures, typically about 900K, the felt pad has a very low yield strength of about $7 \times 10^6$ $N/m^2$†. Consequently, the felt pad is incapable of producing any significant level of stress on the ceramic.

The temperature of the hot-side gas adjacent to the test panel increases as one moves downstream of the cooling slot. This is due to the steady deterioration of the coolant film caused by its interaction with the main flow of hot gases. This axial variation of the hot-side gas temperature can be predicted using an established experimental correlation as described in Appendix A. The results of this prediction are shown in Figure A1.

Although allowable pad temperatures have yet to be established, it seems reasonable to limit the pad temperature to 1160K, the maximum allowable temperature for a number of commonly used combustor liner materials. The felt-ceramic

---

† From data for 35% dense H-875 pad provided by Brunswick Technetics, Deland, Florida.

interface thermocouple, located 50.8mm downstream from the panel leading edge, is common to all panels and is the farthest downstream. Since the hot-side gas temperature increases as one moves downstream of the cooling slot, this thermocouple is expected to register the highest felt-ceramic interface temperature common to all panels. From Appendix A, the hot side gas temperature 50.8mm from the leading edge is 1556K. The panel, however, extends 82.4mm from the leading edge where the gas temperature is 1726K. If this 170K hot gas temperature difference were to be reflected in the felt-ceramic interface and the interface, 82.4mm from the leading edge, was at the allowable maximum of 1160K, then the maximum allowable felt-ceramic interface temperature 50.8mm from the leading edge is 990K. The steady state felt-ceramic interface temperatures for all panels recorded at the 50.8mm station are shown in Table 4, which also identifies the panels that fail the above discussed criterion.

It can be seen from Table 4 that thin ceramics coupled with thick pads yield high felt-ceramic interface temperatures. For the H-875 pad material, the 8% Yttria ceramic panels are preferable compared to their 20% Yttria counterparts, and the 35% pad density is superior compared to the 45% pad density. For the H-534 pad material, the Yttria content of the ceramic and the pad density do not affect the felt-ceramic interface temperatures. Also, most of the panels which have high interface temperatures consist of H-534 pads which implies that the H-875 pad material displays superior thermal conductivity.

Now consider the ceramic layer which is subjected to thermal stresses caused by temperature gradients. These stresses can lead to cracking and eventual deterioration of the panel. The ceramic can fail either by rupture if the stress level is beyond the rupture limit or by fatigue if the ceramic is subjected to stress cycling at stress levels which may be well below the rupture limit. Since no ceramic cracking was evidenced in the four cycles of the screening tests the ceramic stress levels are clearly below the rupture limit. The main failure mode must then be fatigue caused by thermally induced stress cycling. The number of cycles which the ceramic can be subjected to before fatigue failure occurs is inversely proportional to the stress level it is subjected to in each cycle. Since all panels were subjected to the same

combustor conditions, the ceramic stress level is an important parameter in ascertaining the relative life expectancy.

Figure 7 depicts the manner in which the panels are supported. This figure shows that the axial edges of the ceramic layer are constrained by the combustor side walls. Consequently, spanwise thermal expansion of the ceramic will produce only compressive stresses. Since the compressive strength of the ceramic is very high, these stresses are not likely to cause ceramic failure. The spanwise edges of the ceramic, on the other hand, are free to move. In this case, nonuniform thermal expansion due to a temperature differential across the thickness produces both compressive and tensile stresses (see Appendix B). Since ceramics are weak in tension, it is the tensile stress that is critical in determining panel failure or panel fatigue life.

It is shown in Appendix B that the maximum stress level for a free-to-expand layer is proportional to the temperature difference across the layer. The analysis predicts that the maximum stress occurs on both sides of the layer with the colder side in tension and the hotter side in compression. This can be applied to the ceramic part of the panels if the temperature difference across the ceramic layer is known. The procedure in Appendix C provides a means of doing so.

Before applying these results to the test panels, several assumptions must be borne in mind. First, the hot-side gas temperature is not known from direct measurements and can only be predicted from Appendix A. Second, the analyses in Appendices B and C assume that the temperature is a function only of thickness. This is most certainly not valid for the test panels which also experience axial and spanwise temperature variations. Consequently, one is forced to assume local validity of the results of Appendices B and C. Third, the felt-ceramic interface temperature are known only at two, and in four specimens four, points. So the temperature difference across the ceramic can be estimated only at these points. In general, the felt-ceramic temperature can be estimated at any point where a thermocouple exists if material properties are known. However, the thermal conductivity of the felt pad depends not only on the base metal, but also on the pad density and temperature. Unfor-

| PANEL NO. | CERAMIC THICK-NESS (MM) | PAD THICK-NESS (MM) | PAD DENSITY (%)** | PAD MATERIAL | CERAMIC MATERIAL (%Y)*** | FELT-CERAMIC TEMP. (K) | CERAMIC SURFACE TEMP. (K) | TEMP. DIFF-ERENCE (K) |
|---|---|---|---|---|---|---|---|---|
| 16104-11* | 1.91 | 2.54 | 45 | H-875 | 20 | 1072.0 | 1164.4 | 92.4 |
| 16104-23* | 1.91 | 3.81 | 42 | H-534 | 8 | 1050.0 | 1146.8 | 96.8 |
| 16104-36* | 1.91 | 2.54 | 42 | H-534 | 8 | 1012.0 | 1116.5 | 104.5 |
| 16104-19* | 1.91 | 3.81 | 42 | H-534 | 20 | 1010.0 | 1114.9 | 104.9 |
| 16104-21* | 1.91 | 3.81 | 32 | H-534 | 20 | 1003.0 | 1109.4 | 106.4 |
| 16104-42 | 1.91 | 3.81 | 45 | H-875 | 8 | 957.0 | 1072.7 | 115.7 |
| 16104-30 | 1.91 | 2.54 | 32 | H-534 | 8 | 927.0 | 1048.9 | 121.9 |
| 16104-7 | 1.91 | 2.54 | 35 | H-875 | 20 | 921.0 | 1044.1 | 123.1 |
| 16104-14 | 1.91 | 2.54 | 45 | H-875 | 8 | 909.0 | 1034.6 | 125.6 |
| 16104-28 | 1.91 | 2.54 | 32 | H-534 | 20 | 888.0 | 1018.0 | 130.0 |
| 16104-10 | 1.91 | 2.54 | 35 | H-875 | 8 | 873.0 | 1006.1 | 133.1 |
| 16104-17 | 1.91 | 3.81 | 45 | H-875 | 20 | 864.0 | 999.0 | 135.0 |
| 16104-33 | 1.91 | 2.54 | 42 | H-534 | 20 | 774.0 | 927.9 | 153.9 |
| 16104-4 | 1.91 | 3.81 | 35 | H-875 | 20 | 741.0 | 901.9 | 160.9 |
| 16104-35* | 3.3 | 2.54 | 42 | H-534 | 20 | 1002.0 | 1163.0 | 161.0 |
| 16104-18 | 3.3 | 3.81 | 45 | H-875 | 20 | 932.0 | 1114.4 | 182.4 |
| 16104-12 | 3.3 | 2.54 | 45 | H-875 | 20 | 930.0 | 1113.1 | 183.1 |
| 16104-8 | 3.3 | 2.54 | 35 | H-875 | 20 | 922.0 | 1107.5 | 185.5 |
| 16104-5 | 3.3 | 3.81 | 35 | H-875 | 20 | 921.0 | 1106.8 | 185.8 |
| 16104-22 | 3.3 | 3.81 | 32 | H-534 | 20 | 907.0 | 1097.1 | 190 1 |
| 16104-20 | 3.3 | 3.81 | 42 | H-534 | 20 | 872.0 | 1073.0 | 201.0 |
| 16104-29 | 3.3 | 2.54 | 32 | H-534 | 20 | 729 | 974.9 | 245.9 |

* Felt-ceramic interface temperature > 990K

** % Solidity

*** % Yttria in Yttria stabilized Zirconia

TABLE 4. STEADY STATE TEMPERATURE DIFFERENCE ACROSS THE CERAMIC AT THE 50.8MM STATION

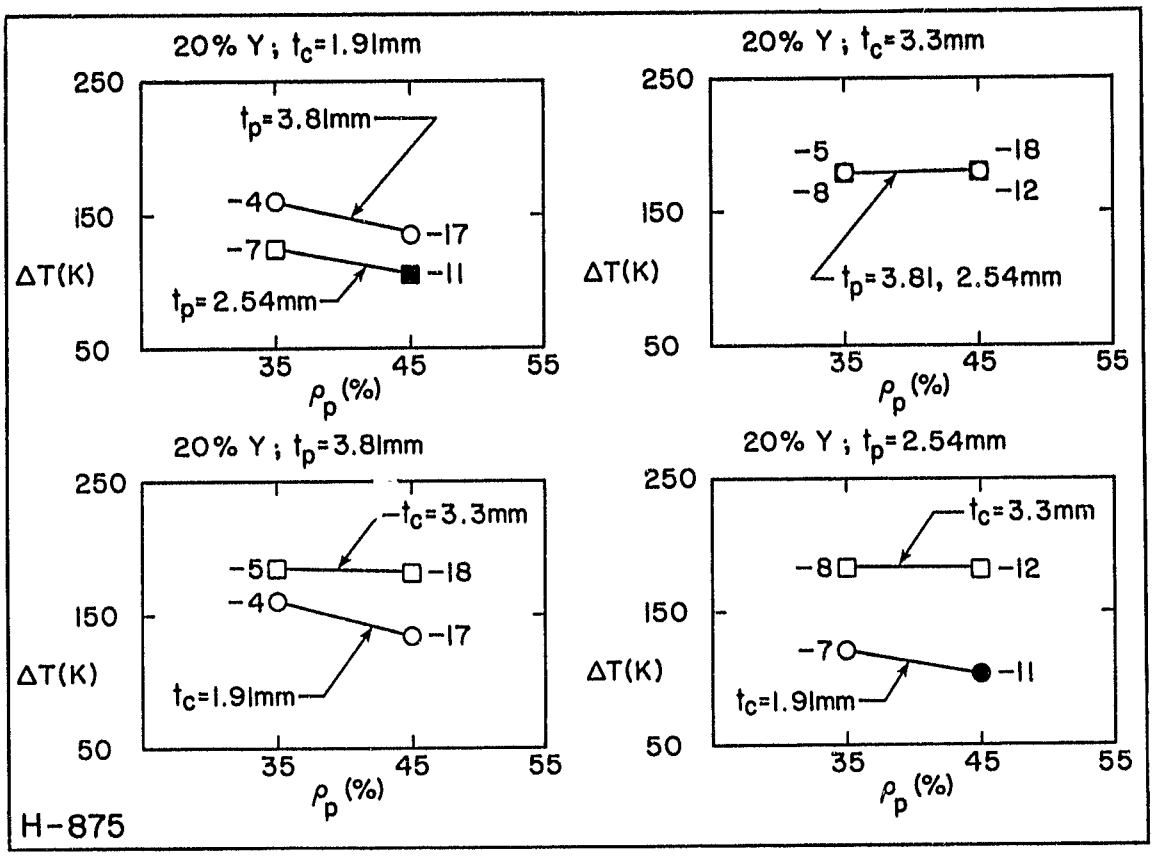


FIGURE 14. EFFECT OF PAD DENSITY ($\rho_p$) ON CERAMIC STRESS LEVEL ($\Delta T$) FOR THE H-875 PAD MATERIAL

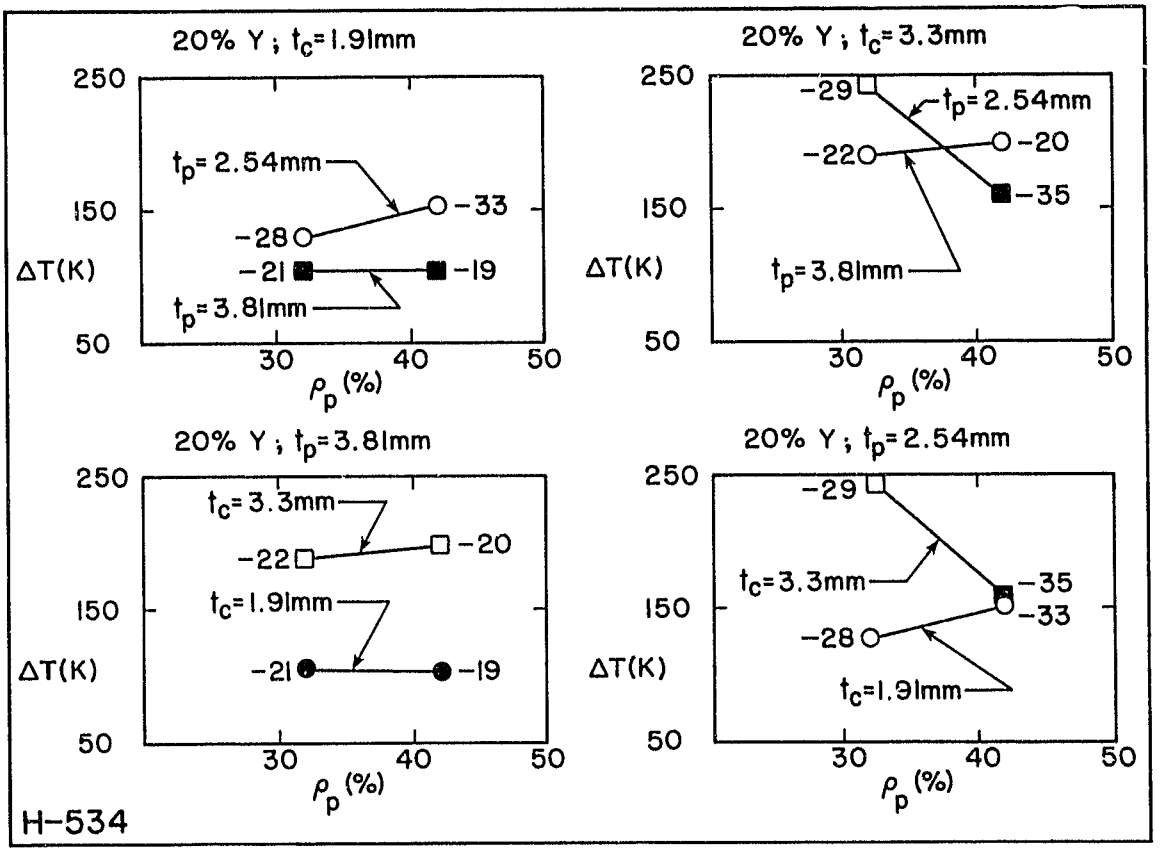


FIGURE 15. EFFECT OF PAD DENSITY ($\rho_p$) ON CERAMIC STRESS LEVEL ($\Delta T$) FOR THE H-534 PAD MATERIAL

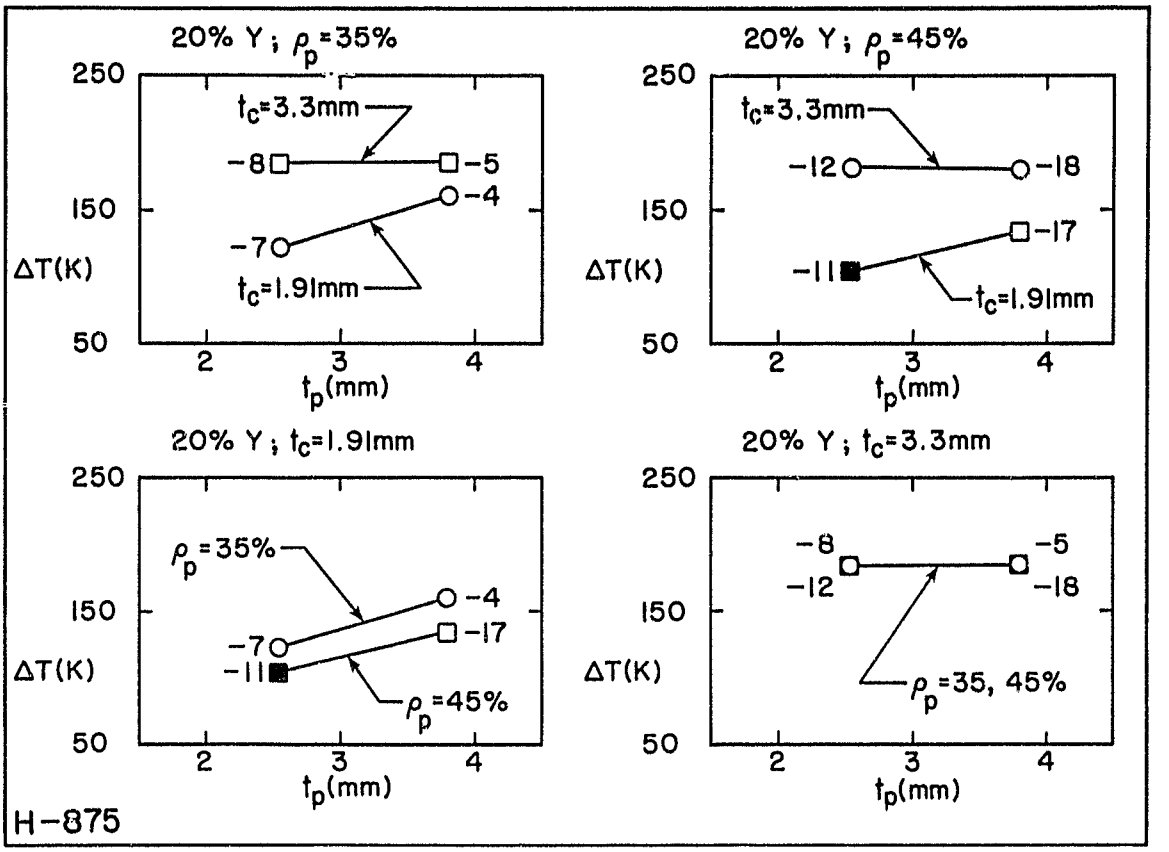


FIGURE 16. EFFECT OF PAD THICKNESS ($t_p$) ON THE CERAMIC STRESS LEVEL (ΔT) FOR THE H-875 PAD MATERIAL

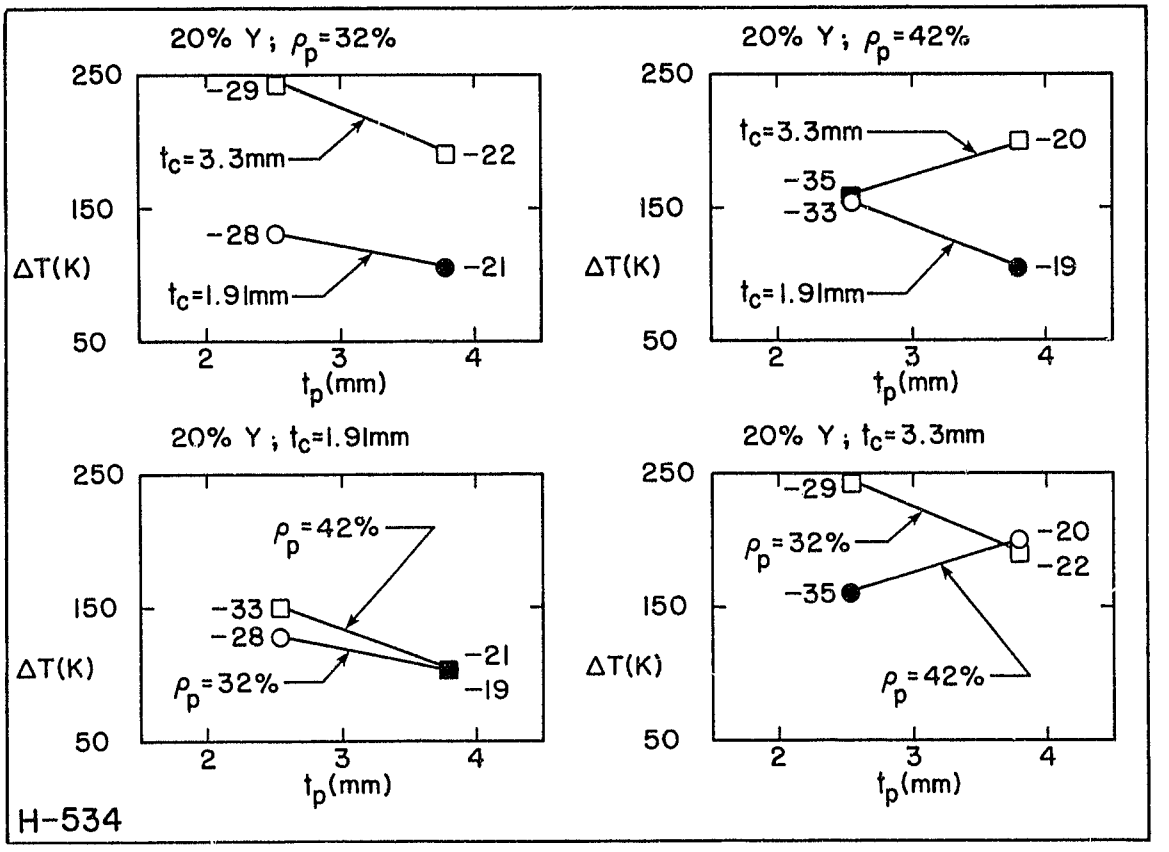


FIGURE 17. EFFECT OF PAD THICKNESS ($t_p$) ON THE CERAMIC STRESS LEVEL (ΔT) FOR THE H-534 PAD MATERIAL

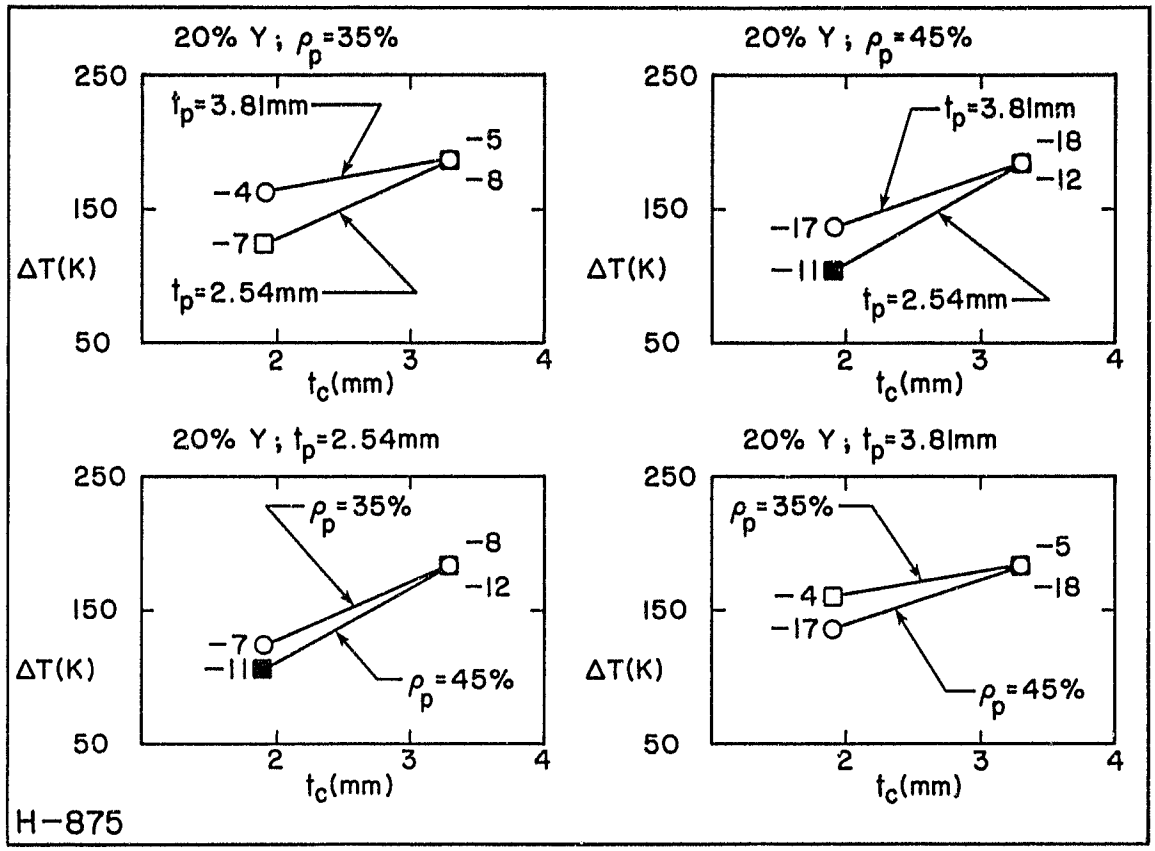


FIGURE 18. EFFECT OF CERAMIC THICKNESS ($t_c$) ON THE CERAMIC STRESS LEVEL (ΔT) FOR THE H-875 PAD MATERIAL

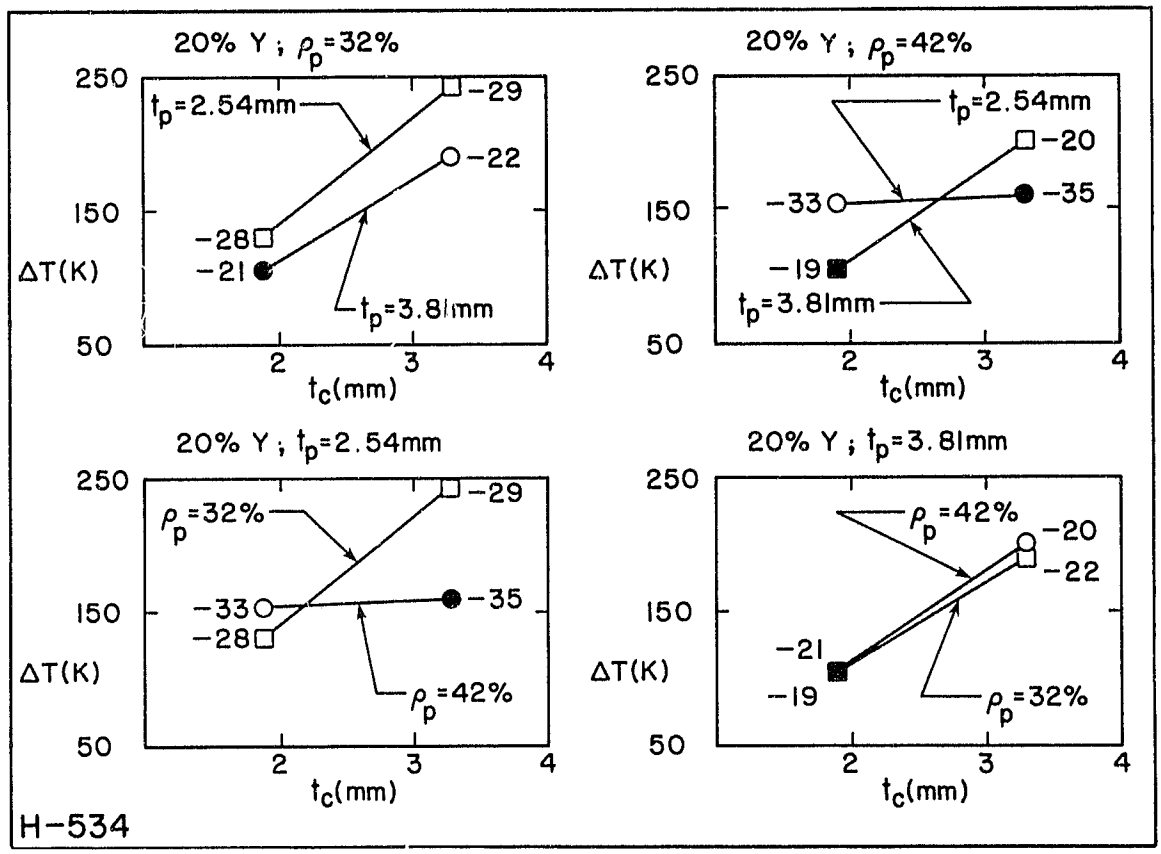


FIGURE 19. EFFECT OF CERAMIC THICKNESS ($t_c$) ON THE CERAMIC STRESS LEVEL (ΔT) FOR THE H-534 PAD MATERIAL

tunately, for the two base metals used, the thermal conductivities have been measured only for a few densities and a limited number of temperatures And, because of the large scatter in the data, interpolation is difficult and yields unreliable estimates. As a result, thermocouples that measure the felt-backing interface temperature or the back surface temperature cannot be used to reliably predict felt-ceramic temperatures. And finally, the results cannot be applied to the transpiration cooled panels.

There are only two felt-ceramic interface thermocouples common to all panels, one 38.1mm and the other 50.8mm from the leading edge. Of the two, the latter always yields a higher temperature difference across the ceramic. Since the maximum stress level is of importance, the second measuring station will be used for comparison. The predicted temperature differences across the ceramic at this location for all panels are listed in Table 4. The order of the panels is in terms of increasing temperature differential, or stress level. Therefore, panels listed at the beginning of the table would be expected to have a greater thermal cycle lifetime than those at the end of the table. These results are also presented in graphical form in Figures 14 through 19. With the prefix 16104 deleted, the panel number corresponding to each data point is shown in these figures. The solid data symbols identify panels with measured felt-ceramic interface temperatures in excess of 990K.

From Figures 14 through 19, several qualitative trends can be observed:

1) Pad density has little effect on the stress level, though a higher pad density yields a slight reduction in stress.
2) For thick ceramic layers, the pad density and thickness have no effect on the stress.
3) For thin ceramic layers, the stress levels increase with increasing pad thickness.
4) Increasing the ceramic thickness causes the stress to increase.

The thermal conductivities of zirconia with varying amount of Yttria are not known. Consequently, a single temperature relation* for the ceramic thermal

* Liebert, C.H., and Gaugher, R.E., "The Significance of Thermal Contact Resistance in Two Layer Thermal - Barrier - Coated Turbine Vanes". Paper presented at the International Conference on Metallurgical Coatings, San Diego, CA, April 21-25 1980.

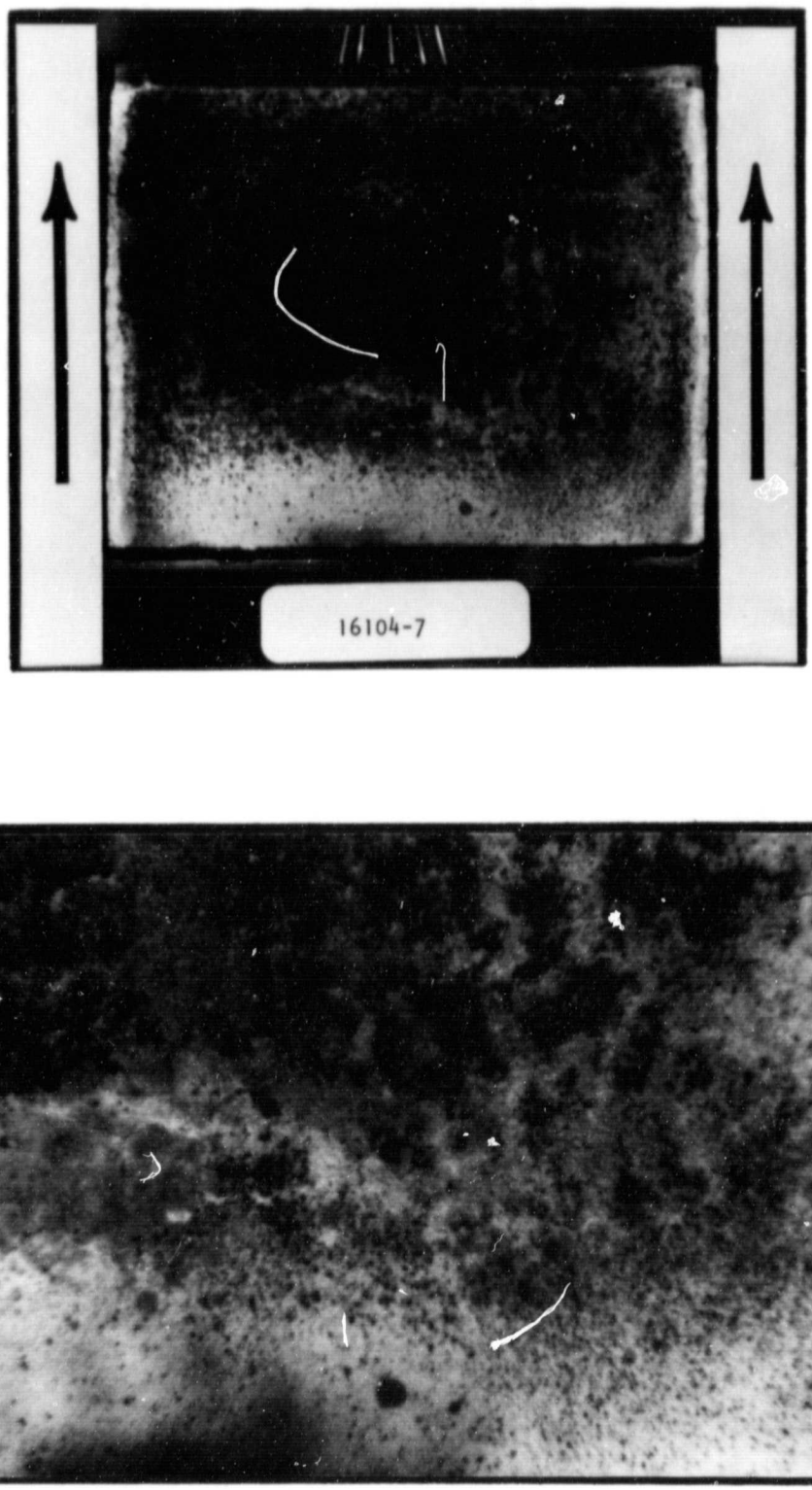


FIGURE 20. CERAMIC SURFACE OF PANEL 16104-7 AFTER ENDURANCE TESTING

ORIGINAL PAGE
COLOR PHOTOGRAPH

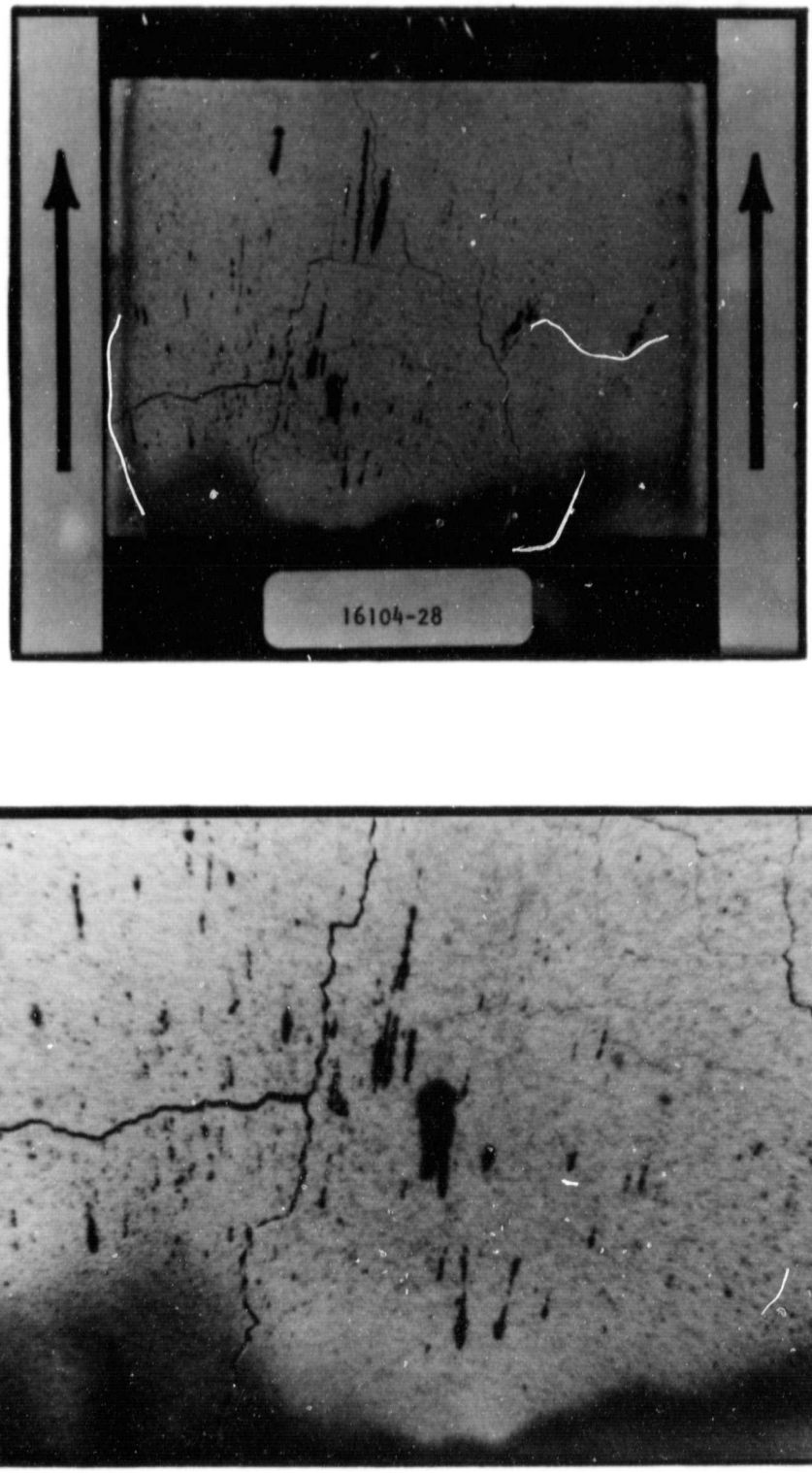


FIGURE 21. CERAMIC SURFACE OF PANEL 16104-28 AFTER ENDURANCE TESTING

conductivity was used for all panels in the foregoing results. This does not alter, in any serious way, the comparative nature of the results. However no conclusions regarding Yttria content in the ceramic can be drawn.

Endurance Tests

After completion of the screening tests, panels #16104-7 and 16104-28 were selected from among the group exhibiting lowest stress levels for further testing to evaluate their endurance characteristics. The selection criteria were low stress levels in panels with approximately the same properties but with different pad materials.

Both panels, #16104-7 and #16104-28 completed the endurance test procedure without structural failure. Panel #16104-7, shown in Figure 20, shows some discoloration of the ceramic and backsurface. A closeup view of the ceramic surface reveals mudflat cracks. These cracks are found over the surface and show no preferential location. The ceramic did not separate from the intermediate felt pad and there is no visible damage to the felt pad, the backing, or the felt-backing interface. The black-grey material seen on the ceramic surface of Figure 20 is the slag deposition from the flameholder burnout noted earlier. It is not likely that this slag deposition could have contributed to ceramic cracking. Most important, the ceramic layer, despite the slight deterioration, was able to protect the metal portions of the panel from damage. This is also true for panel #16104-28 shown in Figure 21. This panel also displays some cracks in the ceramic surface. In addition, some of the ceramic surface at the downstream end of the panel separated from the felt pad. Despite the local separation, the ceramic surface remained attached to the pad and protected the panel from damage.

## CONCLUSIONS

The felt-ceramic composite material has a high degree of survivability in a very high temperature, 2170K combustor environment with very little film cooling. Repeated thermal cycling produced small non-catastrophic cracks in the ceramic coating of one test specimen and caused partial ceramic separation from the felt pad of another test specimen.

The stress level in the ceramic layer, which is related to the fatigue life, is proportional to the temperature difference across the ceramic. Thin ceramics coupled with thin felt pads produce the lowest stress levels. Since this combination also produces high felt-ceramic interface temperatures, there is an optimum combination of ceramic thickness and pad thickness for maximum cycle lifetime. In this preliminary investigation, no quantitative conclusions regarding the effect of various physical properties on the optimum felt-ceramic combination or its fatigue life could be reached.

Felt pad density has little effect on material performance, though a higher pad density slightly reduces the ceramic stress levels. The current lack of data on material properties and the limited number of samples tested here preclude any conclusions regarding favorable ceramic or felt material selection.

# APPENDICES



## A. Hot-Side Adiabatic Wall Temperature:

The adiabatic combustor wall temperature, downstream of a coolant injection slot, is generally described in terms of the cooling effectiveness, $\eta_c$, which is defined as follows:

$$\eta_c = \frac{T_h - T_w}{T_h - T_{cool}} \tag{A1}$$

Since the coolant film constantly interacts with the main effluent of combustion gases, it continually decays as one moves farther downstream. This decay of the coolant film is reflected by a corresponding decrease in $\eta_c$. Tacina and Marek* have shown that the variation of $\eta_c$ is given by

$$\eta_c = 1/(1 + xc_{ph} V_h \rho_h c_m / h_{slot} c_{p_{cool}} V_{cool} \rho_{cool}) \tag{A2}$$

where $c_m$ is the turbulent mixing coefficient, which has a value of 0.05 and is independent of any other parameters.

For the combustor operating conditions in this program,

$$\rho_h V_h A_h = 48\% \text{ of the total air,}$$

and

$$\rho_{cool} V_{cool} A_{cool} = 1\% \text{ of the total air.}$$

Since the width of the combustor and cooling slot are equal, we have,

$$\frac{\rho_h V_h}{\rho_{cool} V_{cool}} = 48 \frac{A_{cool}}{A_h} = 48 \frac{h_{slot}}{h_{comb}} \tag{A3}$$

Substitution of this equation in Equation A2 yields,

$$\eta_c = 1/(1 + xc_{ph}(48)(0.05)/h_{comb} c_{p_{cool}}) \tag{A4}$$

---

*Robert R. Tacina and Cecil J. Marek, "Film Cooling in a Combustor Operating at Fuel-Rich Exit Conditions", NASA TN D-7513, 1974.

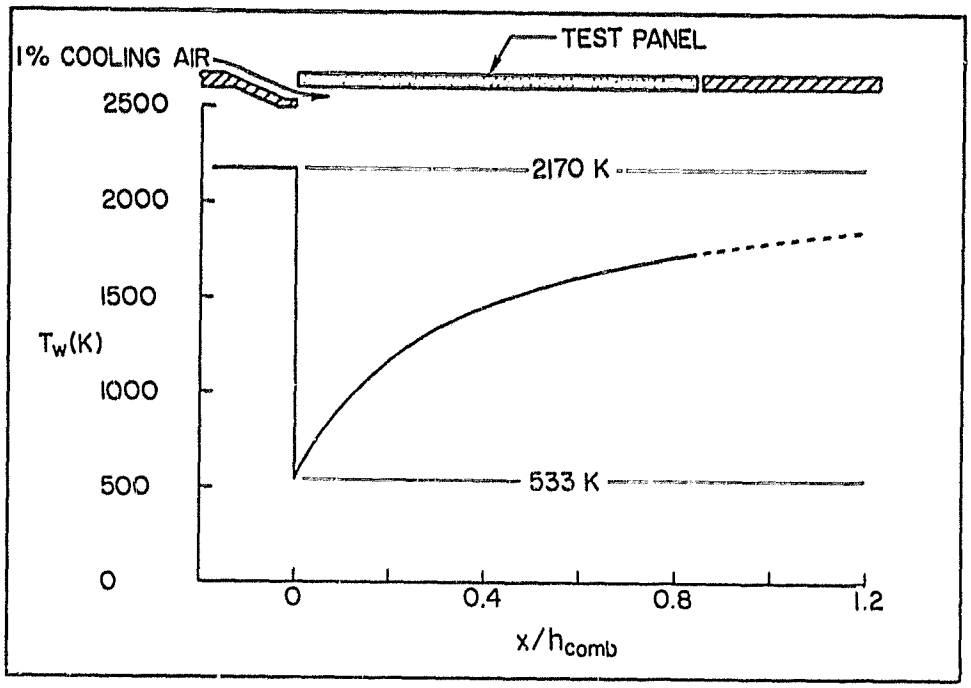


FIGURE A1. AXIAL VARIATION OF ADIABATIC WALL TEMPERATURE.



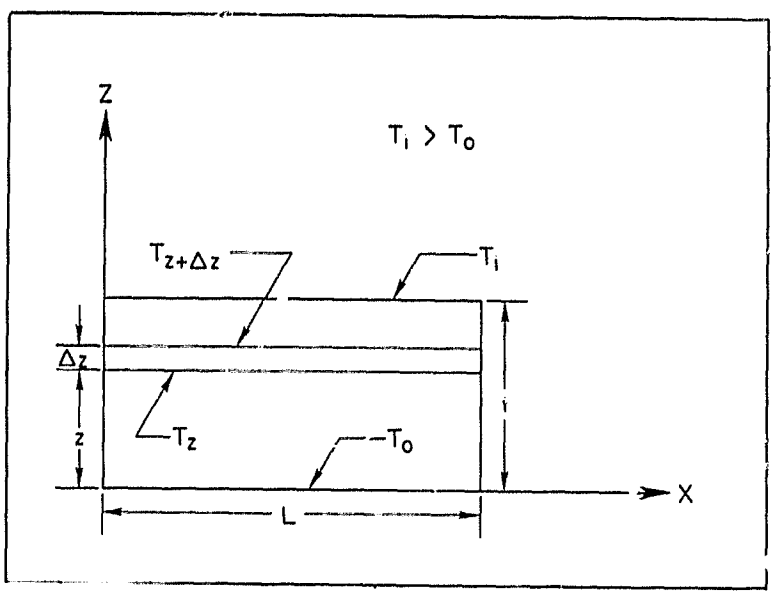


FIGURE B1. COORDINATE SYSTEM FOR THERMAL STRESS ANALYSIS.

where a value of 0.05 has been used for $c_m$. Measurements show that the coolant injection temperature is very nearly equal to the inlet temperature which is nominally 533 K. Also, if the combustion gases are assumed to be at 2170 K, the adiabatic flame temperature, then equation A1 becomes:

$$\eta_c = \frac{2170 - T_w}{2170 - 533} \tag{A5}$$

Furthermore, if air is taken to be the working fluid, then evaluating the constant pressure heat capacities** for the coolant (@ 533K) and hot gas (@ 2170K) yields .247 kcal/kgK and .337 kcal/kgK, respectively. Therefore, equation A4 becomes,

$$\eta_c = 1/(1+.0327x) \tag{A6}$$

where a value of 100 millimeters has been used for $h_{comb}$, the combustor height, and so x must be measured in millimeters. Eliminating $\eta_c$ from equations A5 and A6 we have,

$$T_w = 2170 - 1637/(1+.0327x) \tag{A7}$$

This relation yields $T_w$ = 1556 K at x = 50.8 mm., and $T_w$ = 1726 K at x = 82.2 mm. Equation A7 is plotted in Figure A1 to illustrate the variation of the adiabatic wall temperature downstream of the coolant slot.

B. Thermal Stress:

Consider a layer of material as shown in Figure B1. The layer has a temperature gradient along the z direction, and is free to thermally expand along x. Assuming the temperature gradient is constant we have

$$T_z = T_o + z\,(T_i - T_o)/t$$

---

** Fluid Flow Data Book, General Electric Company, Schenectady, New York.

and



$$T_{z+\Delta z} = T_o + (\Delta z + z)(T_i - T_o)/t$$

If L is unheated length, at temperature $T_{ref}$ , then the thermal expansion of the fiber at z is

$$L\alpha(T_o + z(T_i - T_o) - T_{ref.})/t$$

and that of the fiber at $z + \Delta z$ is,

$$L\alpha(To + (z+\Delta z)(T_i - T_o) - T_{ref})/t$$

Therefore the differential strain, between the two fibers, $\Delta\varepsilon$, is given by

$$\Delta\varepsilon = \Delta z(T_i - T_o)L\alpha/Lt \qquad (B2)$$

And so, the differential stress between the fibers, $\Delta\sigma$, can be written as follows,

$$\Delta\sigma = E\alpha\ \Delta z(T_i - T_o)/t \qquad (B3)$$

Taking the limit as $\Delta z \to o$, we can formally write,

$$\frac{d\sigma}{dz} = E\alpha(T_i - T_o)/t \qquad (B4)$$

Integrating, we have

$$\sigma = \frac{E\sigma(T_i - T_o)}{t}\ z + c \qquad (B5)$$

The constant is evaluated using the fact that,

$$\int_o^t (\sigma x 1)\,dz$$

must equal the external load. In the absence of an external load*

$$c = - \frac{E\alpha(T_i - T_o)}{t} \frac{t}{2}$$

and therefore,

$$\sigma = \frac{E\alpha(T_i - T_o)(z - t/2)}{t} \tag{B6}$$

Applying this to the ceramic layer of the felt ceramic panels we get

$$\sigma_{cer} = \frac{E\alpha(T_{sur} - T_{fc})(z - t_c/2)}{t_c} \tag{B7}$$

and

$$|\sigma_{cer}(max)| = E\alpha(T_{sur} - T_{fc})/2 \tag{B8}$$

Note that the maximum stress occurs at $z = 0$ where the fibers are in tension, and at $z = t_c$ where the fibers are in compression.

C. Temperature Difference Across Ceramic Layer:

The wall temperature, $T_w$, calculated in Appendix A is valid only for an adiabatic wall. For a non-adiabatic wall, $T_w$ is really the gas temperature adjacent to the wall and the wall surface temperature must be estimated by other means. If we assume that all the heat transferred to the wall is conducted through it, then for the ceramic layer of the panels we have,

$$A_{sur}(T_w - T_{sur})\, h_h = [T_{sur} - T_{fc}] \frac{k_{cer} A_{sur}}{t_c} \tag{C1}$$

*For the test panels. The only possible load on the ceramic is the resistance of the felt pad which is very small.

Knowing $k_{cer}$, $t_{cer}$, $h_h$ and $T_{fc}$ the surface temperature $T_{sur}$ can be calculated using $T_w$ of Appendix A. Equation C1 assumes that the temperatures are a function only of the thickness coordinate and that no heat loss from the edges of the ceramic layers are present.



D. Hot Gas Heat Transfer Coefficient

The hot gas heat transfer coefficient, $h_h$, is given by,

$$h_h = \rho_h V_h c_{ph} S_t \quad . \tag{D1}$$

The Stanton number, $S_t$, can be evaluated from the following correlation,*

$$S_t = 0.023(R_e)^{-0.2}(P_r)^{-2/3} \quad . \tag{D2}$$

Assuming the working fluid to be air at 2170 K and 0.5 MPa, Equation D2 can be evaluated for a hot gas flow rate of .40 kg/sec [Table 2] through a cross sectional area of $0.01 m^2$. This yields,**

$$S_t = 0.0031$$

and

$$h_h = \frac{.3984}{0.01} \quad (337).0031 = 174.9 \ W/m^2/K \quad .$$

E. Symbols

$\alpha$ - coefficient of thermal expansion

A - cross sectional area

$c_p$ - constant pressure heat capacity

$c_m$ - turbulent mixing coefficient

$\eta_c$ - cooling effectiveness

E - modulus of elasticity

---

*Welty, James R., Engineering Heat Transfer, John Wiley & Sons, New York, 1974.

**Fluid properties from GE Data Book on heat transfer.

$h_{comb}$ - height of combustor

$h_{slot}$ - hot gas heat transfer coefficient

$k_{cer}$ - ceramic thermal conductivity

$P_r$ - Prandtl number

$R_e$ - Reynolds number

$\rho$ - fluid density

$S_t$ - Stanton number

$t_c$ - ceramic thickness

$T_{cool}$ - film coolant injection temperature

$T_{fc}$ - felt ceramic interface temperature

$T_h$ - hot gas temperature

$T_{sur}$ - ceramic surface temperature

$T_w$ - adiabatic wall temperature

V - velocity

x - axial coordinate measured downstream from cooling slot

z - thickness coordinate

h(subscript) - hot gas quantities

cool(subscript) - slot coolant quantities